Phase separation in yeast vacuole membranes

Chantelle L. Leveille

A dissertation
submitted in partial fulfillment of the
requirements for the degree of

Doctor of Philosophy

University of Washington
2022

Reading Committee:

Sarah L. Keller, Chair
Alexey J. Merz
Dan Fu

Program Authorized to Offer Degree:
Chemistry

© Copyright 2022

Chantelle L. Leveille

University of Washington

Abstract

Phase separation in yeast vacuole membranes

Chantelle L. Leveille

Chair of the Supervisory Committee:

Professor Sarah L. Keller

Department of Chemistry and Physics

Membranes of vacuoles, the lysosomal organelle in yeast, phase separate into two coexisting liquid phases. This phenomenon provides a physical mechanism for lateral organization of biological membranes. Budding yeast is currently the only known living, unperturbed cell system in which reversible, micron-scale phase separation of a membrane has been clearly observed. In this dissertation, I show how the yeast cell adapts and tunes its vacuole membrane to invoke phase separation. If it is important for cells to regulate phase separation of their membranes, then we expect yeast cells to acclimate to external conditions. I measure miscibility transition temperatures of vacuole membranes and find that they scale linearly with the temperature cells are grown at. Then, I purify yeast vacuoles in two growth stages, one in which vacuole membranes phase separate, and the other in which the membranes do not, and, I analyze the lipidome for the membrane. I find that the lipid profile of the vacuole membrane changes dramatically through the growth stages. Melting temperatures have been measured (or can be estimated) for about half of the lipids in vacuole membranes. For this set of lipids, I observe that membranes that phase separate have slightly higher melting temperatures. Overall, this research demonstrates that yeast physiologically adapt to maintain proximity to the transition and identifies key molecular players for membrane phase separation in living cells.

TABLE OF CONTENTS

ACKNOWLEDGEMENTS

Finding the words to describe how grateful I am for the people who have helped me arrive at this point in my scientific career and in my life leaves me in a puddle of tears. I am overwhelmed by the love, passion, and support that have surrounded me. Here, I will do my best to articulate.

Thank you Prof. Sarah Keller for your endless enthusiasm and incredible support. I feel so grateful to have spent the past 5 years in your lab. I hope to be as good of a mentor as you one day. Thank you, Prof. Alex Merz for your mentorship as well. You both are as brilliant of scientists as you are wonderful people and I am so blessed to have worked with you both.

Thank you Caitlin Cornell, who I had the honor of working alongside for many of the experiments you will read about here. You are a fierce, brilliant, scientist and friend. I hold our time at the microscope so close. Thank you to all my labmates Scott Rayermann, Glennis Rayermann, Zack Cohen, and Heid Spears. You made me better and made me laugh everyday.

My dear friends Lizzy Canarie and Sarah Pristash, thank you for getting me through that first year and never letting me go after that. Thank you to Crossfit Deliverance for being my second home and giving me the best gym friends I could ask for. Thank you Sebastian Matt, for giving me the balance rarely achieved by a graduate student—filling my evenings with laughter and fitness and my weekends with adventure and kinship. You celebrated my highs and scooped me up when I was low. Shoulder to shoulder. I am forever grateful.

Thank you to my family, who taught me that I really could do anything I set my mind and my heart to. Thank you to my parents, Teri and Larry, who have supported me wholeheartedly. I stand on their shoulders every day. None of my success would have been possible without their love and support. And to my siblings: Autumn, Carissa, and Dominic who are my biggest fans. They root and cheer me on everyday, and I couldn’t have done it without their encouragement.

CHAPTER 1

Introduction to membranes

Lipids and lipid bilayers

Membranes are two dimensional structures made of molecules called lipids. Lipids are amphiphiles, which means part of their structure is hydrophilic ("water loving") while the other part is hydrophobic ("water fearing") (Fig. 1.1A). Driven by the hydrophobic effect, lipids in water self-assemble into various shapes that minimize contact of the hydrophobic tails with water. One abundant shape is of a lipid bilayer: a sheet of two monolayers with the hydrophobic tails facing inward and the head groups interfacing with the water (Fig. 1.1B). While the lipids are constrained from moving out of the plane of the bilayer, they can freely diffuse laterally within the bilayer and, to a lesser extent, flip from one monolayer to the other.

Phospholipids are composed of a head group attached to a fatty acid carbon tail through a glycerol backbone. Head groups can vary in size and charge, whereas fatty acid chains vary in length and unsaturation (number of double bonds). Another lipid type is a sterol, which is also amphiphilic, and has a small hydroxyl group attached to a rigid ring structure (Fig. 1.1A).

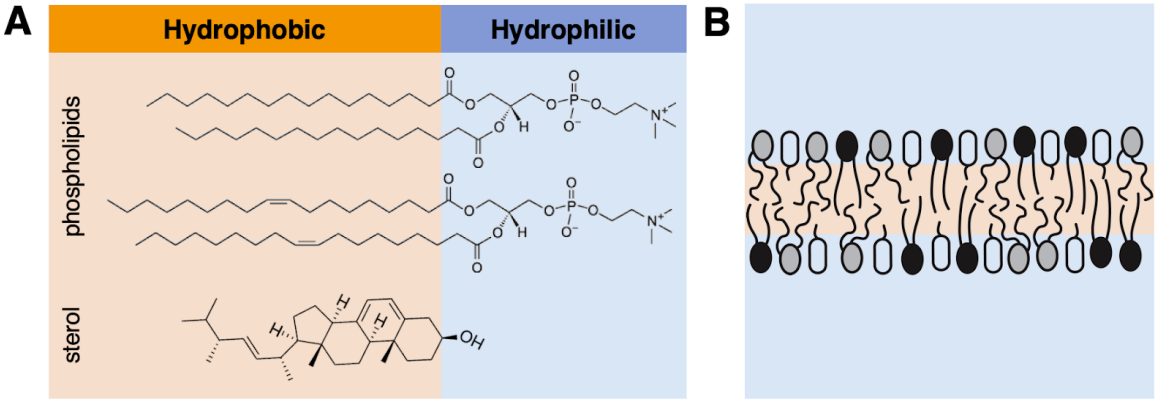

Figure 1.1: (A) Lipids have an amphipathic structure. Phospholipids have a hydrophilic region containing a variable head group attached to a glycerol backbone and a hydrophobic region made up of carbon chains. **Top:** Lipids with saturated acyl chains, like dipalmitoylphosphatidylcholine (DPPC), have a high melting temperature (41°C). **Middle:** Lipids with flexible unsaturated acyl chains, like dioleoylphosphatidylcholine (DOPC) have lower melting temperatures (-17°C). **Bottom:** Sterols, like ergosterol shown here, have a hydroxyl 'head' group and a rigid, planar ring structure. **(B)** When lipids like DOPC, DPPC and sterol are in aqueous solution, they can form a bilayer structure known as a membrane.

Lipids can be characterized by their melting temperature (T_{melt}). For any given head group, this temperature is largely determined by the length and unsaturation of the acyl chains (1). For example, lipids with long, saturated acyl chains (e.g. DPPC) have high melting temperatures (just as saturated cooking fats like butter do) and lipids with short, unsaturated acyl chains (e.g. DOPC) have low melting temperatures (just as unsaturated cooking fats like olive oil do) (Fig. 1.1A). Sterols can have variable effects on phospholipids of different melting temperatures (2–4). For phospholipids that are below their melting temperature, an addition of sterol can disrupt the packing of the lipid's acyl chains, resulting in a "fluidizing" effect. For phospholipids that are above their melting temperature, an addition of sterol can increase the orientational order in the lipid's acyl chains, resulting in a condensing effect.

Membrane phase separation

Lipid bilayers can phase separate into two coexisting liquid phases. This phenomenon has been shown in synthetic membranes containing as few as three lipid types: a high melting temperature lipid, a low melting temperature lipid, and a sterol (Fig. 1.2A) (5–7). At high temperatures, the entropy of mixing all the lipid components increases, and the membrane is mixed in one uniform liquid phase. At low temperatures, the interactions between molecules become more important than the entropy of mixing, and the lipids demix into two coexisting liquid phases (Fig. 1.2B). These two phases are called the "liquid disordered" and the "liquid ordered" phases. The liquid disordered (L_d) phase is enriched in bulkier molecules like unsaturated lipids and fluorescently labeled lipids (8). The liquid ordered (L_o) phase, while still fluid, is enriched in molecules that pack more tightly like saturated lipids and sterols (Fig. 1.1A). It should be noted that while each phase is enriched in particular lipid types, every lipid is present in both phases. The temperature at which the membrane switches from mixed to demixed is called the miscibility transition temperature (T_{mix}) (Fig. 1.2B).

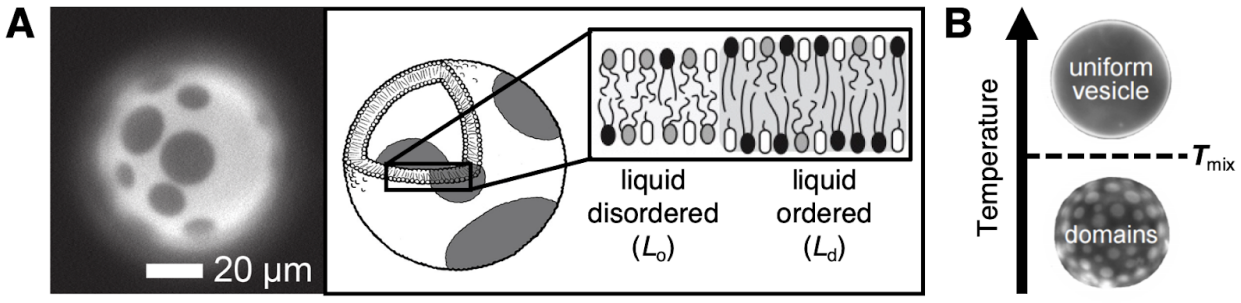

Figure 2: When lipid bilayers form a spherical shell, the resulting shape is called a vesicle. **(A)** The image on the left shows a fluorescence micrograph of a phase-separated giant unilamellar vesicle in aqueous solution. The dark spots are the liquid ordered (L_o) phase enriched in high-T_{melt} lipids and sterol. The bright region is the liquid disordered (L_d) phase enriched in low-T_{melt} lipids. The schematic on the right depicts the distribution of lipids in each of the two phases. In experiments, a fluorescently labeled lipid dye preferentially partitions to the L_d phase, which is why it appears bright. **(B)** When a membrane is above its miscibility transition temperature (T_{mix}), it is uniformly mixed. Below T_{mix}, the membrane demixes. The phase-separated spots on a membrane are often referred to as domains. T_{mix} is the temperature at which the membrane transitions from mixed to demixed.

Membrane phase separation in living cells has been difficult to study. Micron-scale domains had been observed by fluorescence microscopy since 2001 in model membranes ranging in complexity from the simple three component membranes of giant unilamellar vesicles to giant plasma membrane vesicles (which are derived from cells, but no longer a part of the cell) composed of hundreds of lipids and proteins (6, 9, 10). However, there were no direct observations by fluorescence microscopy of micron-scale phase separation in a living, unperturbed cell. Smaller-scale domains may exist in some living membranes; descriptions of lipid rafts treat membrane domains in living cells as submicron, dynamic platforms (11–14). Short-lived, nanoscale domains are challenging to observe using conventional microscopy, leading to skepticism in the field about whether or not living cell membranes contain small-scale rafts, and disagreement about the circumstances that might lead to rafts.

This challenge brings us to the membrane system at the center of the present work: the yeast vacuole. Membranes of vacuoles, the lysosomal organelles of *Saccharomyces cerevisiae* (budding yeast), undergo extraordinary changes during the cell's normal growth cycle. The cycle begins with a stage of rapid cell growth called the logarithmic stage. This "log" stage is followed by the stationary stage, where glucose or other nutrients become limiting, growth slows, and vacuole membranes begin to exhibit micron-scale domains (Fig. 1.3A). Evidence of membrane heterogeneities in yeast vacuoles was first discovered in the early 1960s using freeze fracture electron microscopy, revealing membrane domains depleted of large proteins (15). Studies suggest that these domains are important for yeast survival by acting as docking sites for the metabolism of lipid droplets during periods of starvation (i.e. stationary stage) and by organizing membrane proteins that play key roles in a central signaling pathway conserved among eukaryotes (TORC1) (16–20).

Proof that the domains first observed by freeze fracture (and later fluorescence microscopy) are indeed two coexisting liquid phases was published only recently (21). Like model membranes, vacuole membranes have a characteristic T_{mix} which can be crossed reversibly to mix and demix the membrane (21). The two phases are also enriched in particular lipids and molecules: the L_o phase is enriched in sterols (shown by the binding of the fluorescent dye fillipin) (16), while the L_d phase is composed of bulkier molecules like proteins. In their landmark paper, Toulmay and Prinz tested over a dozen different protein markers on the vacuole, and found that all segregate to one of two domains (16). In this work, the L_d phase is visualized using a fluorescently labeled protein, Vph1-GFP, and the L_o phase is the dark domain (Fig. 1.3B).

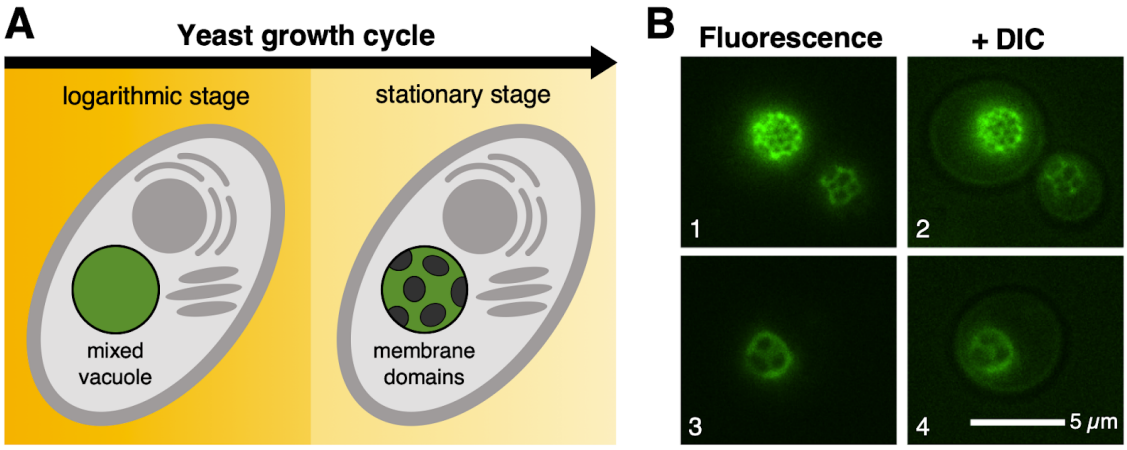

Figure 1.3: (A) Yeast (*S. cerevisiae*) cells have two important stages in their growth cycle. In the logarithmic stage of growth, yeast vacuole membranes appear uniform, in a single liquid phase. In the stationary stage, the vacuole membrane demixes into two liquid phases with compositionally distinct domains. **(B)** Micrographs from Rayermann et al. 2017 show phase-separated yeast vacuoles in the stationary stage. The membrane is labeled with Vph1-GFP and imaged using fluorescence microscopy alone (left column: 1, 3) or using fluorescence microscopy coupled with differential interference contrast (DIC) microscopy (right column: 2, 4) to show the outline of the cell that contains the vacuole.

The yeast vacuole provides a system to answer many outstanding questions in the field about membrane phase separation in a living cell. The research in this dissertation focuses on answering the following questions: If it is important for cells to phase separate, do they regulate phase transitions in response to new physical conditions? What are the key molecules for membrane phase separation in living cells, and how do they compare to the molecular players responsible for membrane phase separation in model systems?

CHAPTER 2

Yeast cells actively tune their membranes to phase separate at temperatures that scale with growth temperatures

This chapter was first published in the Proceedings of the National Academy of Sciences (USA) in 2022 with two modifications: (1) The incorrect citation of Burns et al. 2017 was removed from the sentence "In vitro studies with cell-derived giant plasma membrane vesicles yield similar results: decreasing sterol levels increases Tmix." (2) The following sentence was added "Our results are also consistent with sterol depletion experiments in other cell types" to cite key refencerences Hao et al. 2001 and Mahammad et al. 2010. Changes can be found on pg. 20.

The research in this chapter was conducted in collaboration with C.E. Cornell, A.J. Merz, and S.L. Keller.

INTRODUCTION

Spatial organization of cellular components is essential for their biological function. One way that cells may achieve this organization is through spontaneous demixing of components into coexisting liquid phases. For example, 3-dimensional subcellular condensates or droplets contain proteins and/or RNA at concentrations that differ from the rest of the solution (reviewed in (22–26)). Similarly, 2-dimensional, micron-scale domains in model membranes contain lipids in ratios that differ from the rest of the membrane, independent of whether the membranes are composed of very few lipid types or are derived directly from cells (9, 10).

To date, yeast (*S. cerevisiae*) are the only unperturbed, living cell system in which reversible, micron-scale phase separation of a membrane has been observed. Specifically, domains disappear in individual yeast vacuoles above a characteristic temperature (T_{mix}) and reappear below that temperature. Moreover, domains merge with one another on time scales characteristic of liquid membranes (21). This phase separation had been previously hypothesized (16, 27) and appears to regulate the cell's metabolic response to nutrient limitation through the TORC1 (Target Of Rapamycin Complex 1) pathway that is a central regulator of protein synthesis, autophagy, docking of lipid droplets, and many other processes (16–20). Depletion of nutrients from the growth medium induces yeast to transition from exponential growth (called the logarithmic or "log" stage) to a stage in which cell division slows and the density of the cell culture plateaus (called the stationary stage, Fig. 2.1). When yeast enter the stationary stage, domains that segregate lipids and proteins appear on vacuole membranes, as

observed by both freeze-fracture electron microscopy (15, 28) and fluorescence microscopy (16, 19). Immunogold labeling proves that domains seen by the two methods are the same (29).

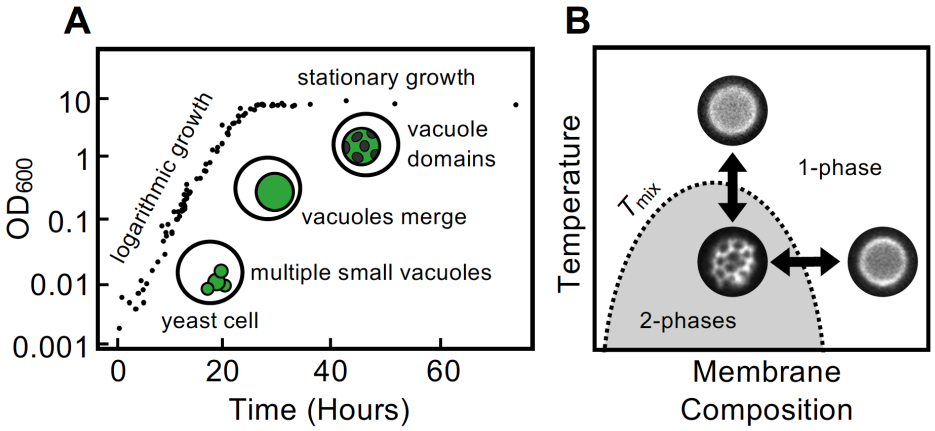

Figure 2.1: (A) Growth curve for *S. cerevisiae* (adapted from Rayermann et al. 2017), where OD600 is the optical density at λ = 600 nm plotted on a log scale. In the logarithmic stage of growth, yeast vacuole membranes appear uniform, in a single liquid phase. Late in the log stage, vacuoles fuse so that most cells contain only one large vacuole. In the stationary stage, the vacuole membrane demixes into two liquid phases with compositionally distinct domains. **(B)** The phase boundary between mixed (1-phase) and demixed (2-phase) states can be reversibly crossed by changes in temperature and/or membrane composition. T_{mix}, the temperature at which membrane domains appear or disappear, changes with membrane composition. Micrographs show representative images of membranes with and without domains (and are not all from the same vacuole).

The clear connection between membrane domains and growth stage makes yeast an ideal system to investigate in order to answer significant open questions about phase separation. Here, we focus on two outstanding questions. First, do yeast cells physiologically adapt to maintain membrane phase separation under new physical conditions? Second, is phase separation induced or eliminated through manipulation of sterol levels?

It is reasonable to expect that yeast should actively remodel their vacuole membranes to achieve phase separation, because domains appear and disappear with growth stage and because yeast adjust to a wide range of environmental conditions (30, 31). More broadly, it is known that many cell types alter their lipid compositions and membrane behaviors in response to changes in cell cycle (32–37), activation (38, 39), disease (40–42), and environmental stress (43). Changes in growth temperature are particularly compelling to investigate because they are

experimentally tractable and because they trigger active membrane remodeling in organisms ranging from bacteria to vertebrate animals (44–47).

If liquid-liquid membrane phase separation is a functionally relevant property, a clear prediction is that the membrane's T_{mix} should be regulated by the cell in response to the ambient temperature. There is some precedent for this. Giant plasma membrane vesicles that are shed from zebrafish cells exhibit fluctuating domains indicative of a miscibility critical point, and the T_{mix} values of these cell-free membranes vary with the growth temperature of the cells that shed them (47). However, there are key differences between plasma membrane vesicles and yeast vacuoles, beyond the fact that one is cell-free and the other is in a living cell. To date, the T_{mix} of all plasma membrane vesicles has been found to be below the cells' growth temperature (10). In these vesicles, an offset between T_{mix} and the growth temperature is hypothesized to set the size of submicron membrane fluctuations, which could in turn influence channel activities and cytoskeletal compartmentalization (48–50). In contrast, the T_{mix} in living yeast vacuoles is well above the growth temperature (21), such that vacuole membranes partition into micron-scale domains under normal conditions. In yeast, it is less clear why a specific offset would be worth regulating: any T_{mix} above the growth temperature should produce large domains in vacuole membranes. However, by regulating an offset, yeast might avoid "burning their bridges", facilitating a return to a uniform membrane.

Of course, yeast cells cannot regulate domain formation by controlling their own temperature. Instead, they must alter the molecules in their membranes. Asking whether yeast tightly control their membrane's T_{mix} is the same as asking whether they tightly control their lipid and protein compositions in the stationary stage (Fig. 2.1B). The detailed mechanisms by which cells adapt their membrane compositions to invoke phase separation in the stationary phase is unknown. In model membranes, coexisting liquid phases appear at intermediate sterol levels (rather than at low or high levels) (4, 9, 51–54). In yeast cells, there are many indications that sterol levels are important. Experiments that alter genes encoding proteins involved in sterol synthesis or transport (17–19, 29), that perturb lipid droplets (which are rich in sterol esters) (19, 20), and that manipulate sterol metabolism (16, 55) all support the hypothesis that sterols regulate the formation and maintenance of membrane domains. However, it is largely unknown in which direction sterols are being shuttled—to or from the vacuole membrane.

In order to address some of these outstanding questions, we investigated whether living yeast cells adjust the T_{mix} of their vacuole membranes to scale with the growth temperature of the cells, and we test whether vacuole domains appear or disappear when ergosterol levels are changed in isolated vacuole membranes.

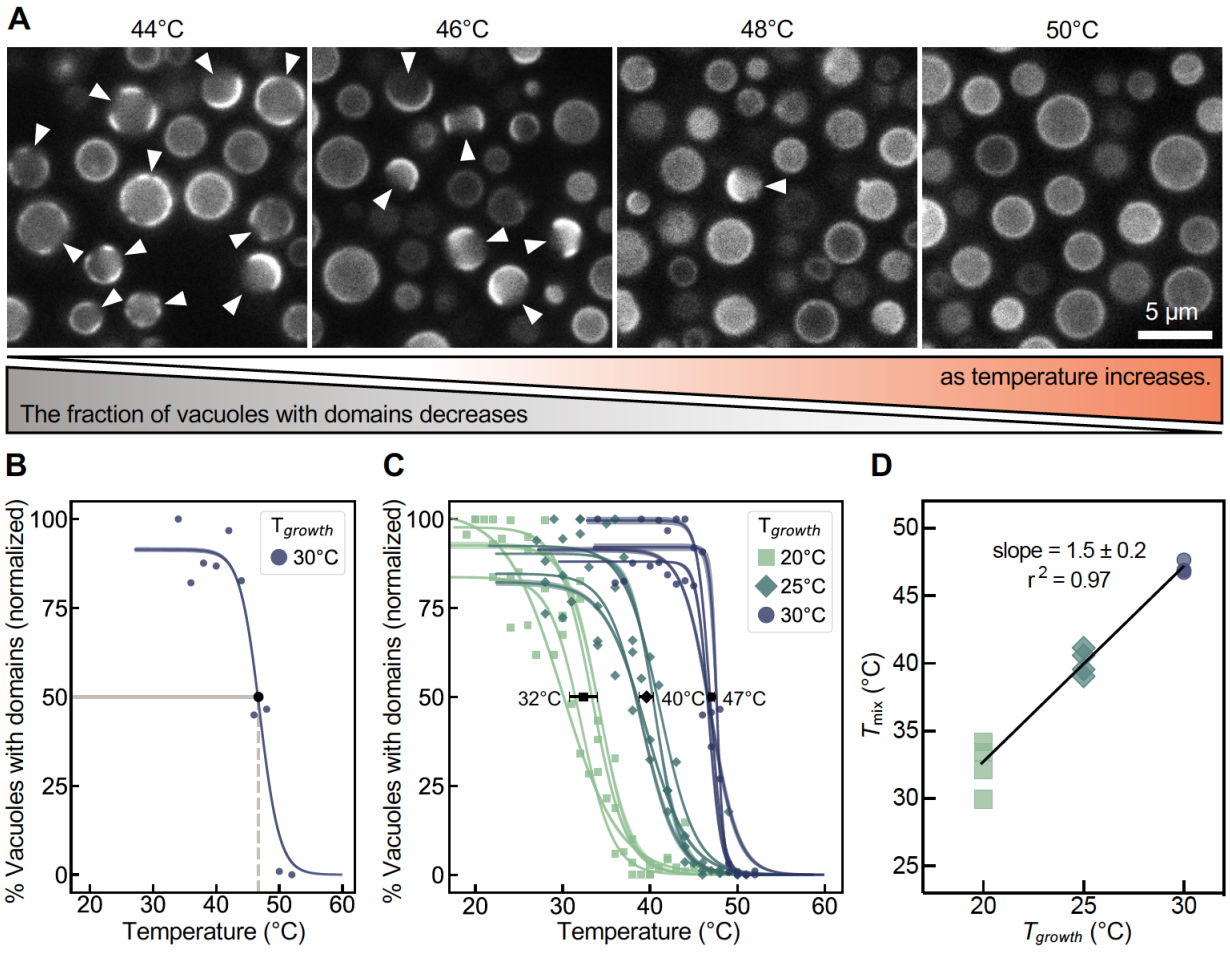

Figure 2.2: (A) Micrographs of vacuoles in living cells at 44°C, 46°C, 48°C, and 50°C, in four different fields of view. At low temperatures, most vacuole membranes are phase separated, whereas at high temperatures, most membranes appear uniform. Arrowheads point to vacuoles with domains, which are identified by contrast between bright and dark regions in the membrane. **(B)** Vacuole membranes in living cells have a characteristic miscibility transition temperature, T_{mix}. This plot represents a single experimental sweep with 2°C steps for cells grown at 30°C. The percent of vacuoles with visible domains (small circles; n = 235 to 466) was scored using a semi-automated blind procedure, normalized to a maximum of 100%, and fit to a sigmoidal curve (see Methods and Fig. 2.S5). The large black circle lies at T_{mix} = 46.9°C, the temperature at which the percent of vacuoles with domains is reduced by 50%. The shaded region superimposed on the line indicates the 95% confidence interval for the fit. **(C)** Increases in growth temperature (20°C, 25°C, and 30°C) result in increases in T_{mix} (32.4 ± 1.6°C, 40.1 ± 0.8°C, and 47.0 ± 0.4°C, where error bars are standard deviations). Each curve

represents a different experimental temperature sweep. (D) The relationship between T_{mix} and the growth temperature is linear. The error in the slope is the 95% confidence interval for the linear regression fit. Offsets (ΔT) between the three growth temperatures and T_{mix} are 12.4 ± 1.6°C, 15.1 ± 0.8°C, and 17.0 ± 0.4°C. Optical densities were controlled to account for changes in growth rate at different growth temperatures (Fig. 2.S1 and Methods).

RESULTS

In previous experiments (21), we investigated a relatively small number of individual vacuole membranes, both within and isolated from living cells. Here, we investigate large populations of cells. Three scenarios are possible. (1) If phase separation is physiologically irrelevant, then we would predict that T_{mix} is not stringently regulated: different cells within a population should exhibit T_{mix} values that range widely above and below the growth temperature. (2) If phase separation is functionally important, and the only constraint is that the vacuole membrane must phase separate in the stationary phase, then we might predict that membranes from different cells should have a wide range of T_{mix} values, as long as T_{mix} is usually higher than the growth temperature. (3) However, if phase separation is functionally important, and if the phase transition must be easily reversed when nutrient conditions change, then we would predict that T_{mix} is tightly regulated, and that the distribution of T_{mix} values should exhibit low cell-to-cell variation across the population.

Yeast vacuoles exhibit a characteristic T_{mix}

Vacuoles in living yeast cells were imaged as in Fig. 2.2A. The bright areas of the membranes are labeled with Vph1-GFP. Vph1 localizes exclusively to the vacuole membrane and is a transmembrane subunit of the V-ATPase pump. We chose Vph1 because it preferentially partitions to liquid disordered domains in phase-separated vacuoles (16, 29, 56). The protein's function, which is to pump protons into the vacuole lumen to generate an electrochemical gradient across the membrane, is not affected by the probe (57). At temperatures below T_{mix}, Vph1 is unevenly distributed in vacuole membranes (marked with arrowheads in Fig. 2.2A), whereas above T_{mix} the membranes appear uniform. To obtain the data in each experiment, multiple fields of view as in Fig. 2.2A were analyzed with a semi-automated, blinded procedure. For a population of cells, T_{mix} is the temperature at which the percent of vacuoles with domains is reduced by 50%. For the single experiment in Fig. 2.2B, each data point represents hundreds of vacuoles in living yeast cells grown at their optimal growth temperature of 30°C.

In turn, multiple experiments as in Fig. 2.2B were combined to generate Fig. 2.2C. We find that the broad population of vacuoles grown at 30°C has a characteristic T_{mix} (47.0°C) with a low variance (standard deviation ±0.4°C). Because T_{mix} is a function of the membrane's composition, the sharp transition implies that there is relatively little cell-to-cell variation in vacuole membrane composition with respect to molecules that control phase separation, even among different yeast cultures. The reproducibility of this result rivals those of chemically defined artificial lipid systems like giant unilamellar vesicles (4, 58). In summary, yeast regulate their vacuole membrane composition to achieve a common T_{mix}, which is set above the ambient growth temperature.

Growth temperature controls T_{mix}

Next, we tested whether cells actively tune T_{mix} of their vacuole membranes in response to changes in ambient growth temperature. We chose the new growth temperatures to be low (20°C and 25°C) rather than high to avoid subjecting cells to chronic thermal stress. Yeast grow robustly at all temperatures tested (Fig. 2.S1 and Methods).

The results, shown in Fig. 2.2C and 2.2D, indicate that yeast maintain a linear relationship between T_{mix} in vacuole membranes and the growth temperature. An increase in the ambient temperature of ~15°C causes membrane components to mix into a single phase. Taken together, the low cell-to-cell variation of T_{mix} and the linear relationship between T_{mix} and the growth temperature strongly support the conclusion that vacuole membrane demixing is stringently regulated and, therefore, physiologically important. Yeast would achieve a shift in T_{mix} through a change in the vacuole's composition.

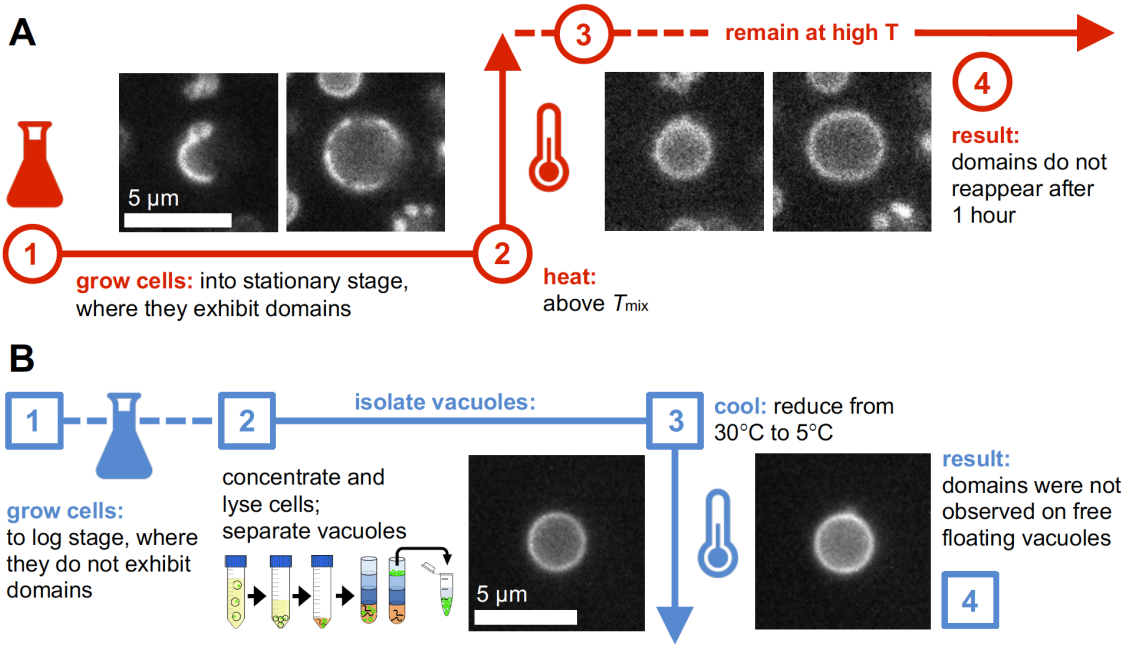

Figure 2.3: (A) Cells adapt T_{mix} of their membranes on timescales longer than 1 hour in response to temperature changes. Cells were grown at low temperature (~20˚C) until they reached the stationary stage, where vacuole membranes exhibited domains. Temperature was then quickly raised to 35˚C (slightly above T_{mix}), and domains disappeared. Cells were maintained at this new temperature for 1 hour; domains did not reappear within this period. Images in Steps 1 and 4 show the same vacuoles; Fig. S2 shows a time lapse. **(B)** Membranes of free-floating vacuoles isolated from cells in the log stage do not phase separate, even at low temperature. Cells were grown at 30˚C to the log stage (OD_{600} = 1). Vacuoles were isolated from these cells and imaged. When the vacuoles were cooled from 30˚C to 5˚C, domains did not appear in the membranes. Images in Steps 3 and 4 show two different vacuoles that are representative of the population.

Membranes require long-term changes in temperature to remodel

Next, we investigated the time scales over which temperature changes regulate domain formation. Previous results indicate that the relevant window falls between 5 minutes and 3 hours. The shorter time scale derives from our previous report that domains do not reappear in vacuoles held above T_{mix} for 5 minutes (21). The longer time comes from the observation that domains eventually appear in log stage vacuoles subjected to 3 hours of acute heat stress (16). We grew cells at low temperature (20°C) until they reached stationary stage and their vacuoles exhibited domains (Fig. 2.3). We then raised the temperature slightly above T_{mix} (35°C). We maintained the cells at this new temperature for 1 hour. Within this period, vacuole membranes did not return to a phase-separated state. Therefore, the time required for significant remodeling of the membranes is > 1 hour. We designed our experiment to avoid heat stress by choosing an initial low temperature (20°C), which resulted in a low T_{mix} (32.4 ± 1.6°C). At the conclusion of

the experiment, cells were cooled back to 20°C, and domains reappeared on vacuoles that originally exhibited them (Fig. 2.S2). We previously showed that miscibility transitions in vacuoles are reversible after acute changes in temperature on time scales of seconds (21). Here we show that the transition is also reversible on a long time scale, suggesting that T_{mix} is regulated in response to a time-averaged growth temperature, rather than *via* rapid cellular responses to acute temperature fluctuations.

Logarithmic stage vacuoles do not phase separate, even at low temperature

As yeast progress from the log stage to the stationary stage, their vacuole membranes demix into two phases. This transition must be driven by a change in the membrane composition, but what is the magnitude of that change? If log stage yeast require only a small change in the composition of their vacuole membranes to phase separate, then only a small drop in temperature should have the same effect. In Fig. 2.3B, we find that even a large drop in temperature (from 30°C to 5°C) does not cause log stage vacuole membranes to phase separate, implying that the membranes undergo a large change in composition from log to stationary phase. For this experiment, we used isolated vacuoles that were fused to ~4 μm diameter because phase separation can be difficult to identify in smaller (~1-2 μm) *in vivo* log stage vacuoles and because isolation does not appear to perturb phase separation (16, 21, 27). We imaged vacuoles that were free-floating rather than resting on the coverslip because it is known that contact between membranes and surfaces can promote membrane phase separation (59–61). Indeed, contact between isolated vacuoles and glass surfaces occasionally caused domains to appear in very cold (5°C) membranes (Fig. 2.S3).

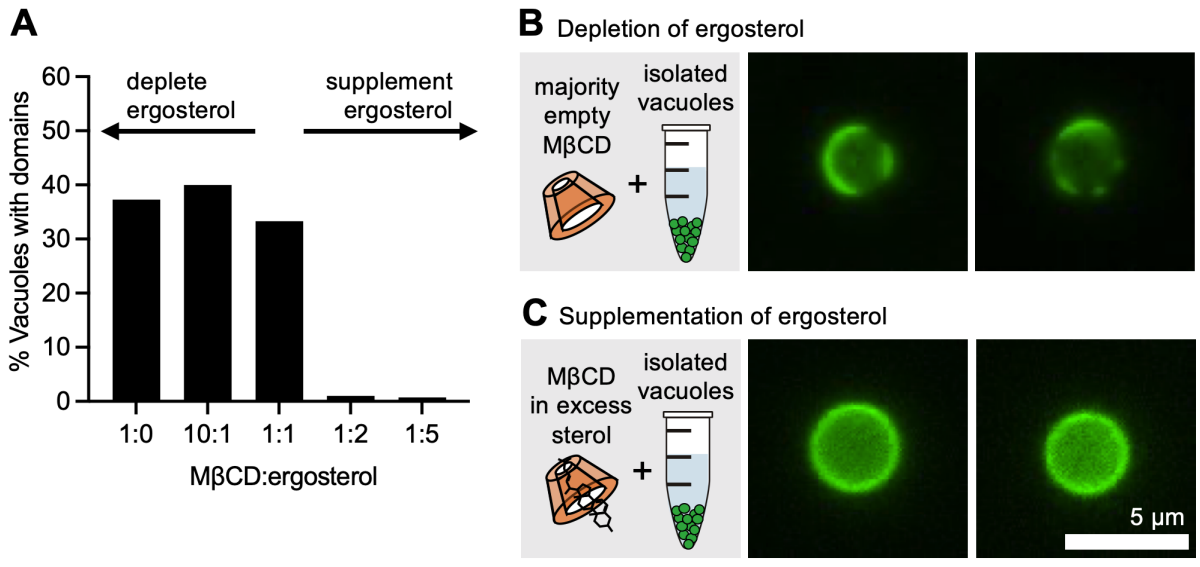

Figure 2.4: (A) In wild-type conditions, log stage vacuoles do not exhibit domains (Fig. 1B). Depletion of ergosterol from vacuoles isolated from log stage yeast triggers membrane phase separation, whereas supplementation of ergosterol has no effect. For each condition, 75 to 141 vacuoles were evaluated. **(B)** Micrographs show dark domains in isolated vacuoles in which ergosterol was depleted by introducing an excess of empty MβCD (as a 10:1 ratio of MβCD:ergosterol). Additional images are in Fig. S4. **(C)** Micrographs show a lack of micron-scale domains in isolated vacuoles in which ergosterol was supplemented by introducing loaded MβCD (as a 1:2 ratio of MβCD:ergosterol).

Depletion of ergosterol causes domains in log stage vacuole membranes

In model membranes, coexisting liquid phases form when the membranes contain moderate amounts of sterol. If the sterol content is low, solid (gel) domains appear; if the sterol content is high, the membrane is uniform (4, 9, 51–54). Given that no domains appear in membranes of log stage vacuoles, one reasonable hypothesis is that their sterol content is too high to support phase separation. In this scenario, a decrease in the sterol content of log stage vacuole membranes would cause coexisting liquid phases to appear. In yeast, the predominant sterol is ergosterol; it constitutes roughly 7-15 mole % of lipids in mid- or late-log stage vacuolar membranes (62, 63). In Table S1, we show that depleting ergosterol in model membranes of giant unilamellar vesicles can indeed increase T_{mix}, whereas supplementing ergosterol can decrease T_{mix}.

We tested our hypothesis by decreasing or increasing the amount of ergosterol in isolated log stage vacuoles fused to ~4 μm diameter. To directly tune the membrane's ergosterol content, we used methyl-β-cyclodextrin (MβCD) as a molecular shuttle to remove and add ergosterol. We found that a decrease in membrane ergosterol caused domains to appear in ~40% of log stage vacuoles, whereas an increase had no effect (Fig. 2.4). The result is robust across several ratios of MβCD:ergosterol, showing that both gentle and stringent methods of ergosterol depletion are effective. Contact between membranes and surfaces can promote membrane phase separation (59–61), and when vacuoles rested on glass, domains nucleated at that surface if ergosterol was depleted, but not if ergosterol was supplemented.

DISCUSSION

Phase separation in living cells

Cells expend energy to maintain molecular fluxes and concentration gradients far from equilibrium. A common question that arises about phase separation is how it can apply to living cells given that it is a classic equilibrium phenomenon. The apparent contradiction is reconciled

if there is a clear separation of time scales. As an analogy, consider a 1 liter aqueous solution in an open beaker on a benchtop. Imagine that reactions in the aqueous solution reach equilibrium quickly (e.g., <1 minute). If we make a change to the solution on a similarly short time scale (e.g., a temperature jump from 25˚C to 37˚C), then we can approximate that the solution will reach a new equilibrium position within about a minute. We can confidently apply equilibrium concepts to our system over intermediate measurement periods (e.g., 1 hour), even though we are aware that if we continued to observe the solution over days, the equilibrium position would continue to very slowly change due to evaporation.

Vacuole membranes exhibit this same separation of time scales, which means that we can apply equilibrium concepts to the membranes over appropriate periods of time. Phase separation reversibly occurs on short time scales, within seconds of the temperature crossing T_{mix} (21). In contrast, the membrane's T_{mix} (or, equivalently, its composition) remains constant over time scales exceeding an hour, within measurement uncertainty (Fig 2.3A). If we continued to observe vacuole membranes over longer times, we would expect the equilibrium position to change due to membrane remodeling. Other examples in which equilibrium phase transitions are applied to living cells include subcellular condensates of proteins and/or RNA, which also exhibit a separation of time scales (22, 23, 25, 26).

Time scales are also invoked in the classification of membrane domains. "Lipid rafts" are typically described as small (nm-scale), short-lived, dynamic platforms in plasma membranes (12, 64–67), unlike the large (μm-scale), long-lived domains seen in vacuole membranes. Of course, phase separation could underlie features attributed to rafts, such as segregating membrane components or influencing protein sorting and function (11, 13, 14, 65).

The role of sterols in membrane phase separation

Here, we probed membrane composition by altering levels of only ergosterol, the major sterol in yeast. We changed sterol levels while keeping all other lipids constant by using MβCD and by isolating vacuoles from other types of membranes that could act as sources or sinks of sterols. We discovered that depletion of ergosterol causes log stage vacuole membranes to phase separate.

Our experiments with vacuoles are consistent with results from artificial membranes. For many ratios of lipids in model 3-component membranes, decreasing the sterol concentration is

equivalent to traveling left along the horizontal arrow in Fig. 2.1B: domains nucleate and T_{mix} increases (e.g. (9, 53, 54)). A higher T_{mix} implies that a broader range of lipid compositions produces coexisting liquid phases (Fig. 2.1B). *In vitro* studies with cell-derived giant plasma membrane vesicles yield similar results: decreasing sterol levels increases T_{mix} (68). *In vitro* experiments with whole-cell lysates are more challenging to interpret. For example, Toulmay & Prinz reported that domains appear on log stage vacuoles in lysates exposed to MβCD. Although their result agrees with ours, they surmised that MβCD was transferring sterols from other membranes in the lysate to vacuoles (16). Likewise, they found that MβCD caused domains to disappear from stationary-stage vacuoles (16), but it was not known if ergosterol was being transferred to or from the vacuoles. Our results are also consistent with sterol depletion experiments in other cell types (69, 70).

Experiments that allow several lipid types to vary at once are similarly challenging to interpret. The list of lipids in yeast membranes is long and diverse, and changes in ergosterol levels could work in concert with (or against) changes in the rest of the lipidome to form membrane domains (71, 72). Most *in vivo* experiments imply that ergosterol levels in vacuoles increase as yeast enter the stationary stage. For example, Tsuji et al. (29) report that filipin staining of sterols in stationary-stage membranes is higher than in log stage, with the caveat that staining was relative to the plasma membrane rather than absolute. Similarly, genetic impairment of sterol synthesis and transport (11–13, 17), perturbations to lipid droplets (which are rich in sterol esters (13, 14)), and the application of drugs to manipulate sterols (10, 44) can prevent the formation or maintenance of domains. However, in many of these processes, the net direction in which sterols are being transferred is unknown. Proof that vacuole phase separation in intact cells always follows an increase in ergosterol would be consistent with the observation that maintenance of phase separation requires lipophagy, which is expected to mobilize esterified sterols stored in lipid droplets (19, 20, 29, 73). Sterol transport may also occur at sites where vacuole makes contact with the ER or other organelles (55). We are currently conducting experiments with purified vacuole membranes to learn how their lipidome remodels over the cellular growth cycle.

Regulation of T_{mix}

Our finding that the T_{mix} of yeast vacuole membranes is tightly regulated in response to ambient growth temperature is consistent with the hypothesis that phase separation is functionally important. This leads to an important question: what downstream biological activities

depend on the formation of phase-separated domains at the vacuole? Domains in vacuole membranes segregate protein complexes of the TORC1 nutrient sensing pathway, which regulates autophagy (16–18). In addition, vacuole domains appear to be necessary for the docking and consumption of lipid droplets, a process called lipophagy (19, 20, 29, 73). Both autophagy and lipophagy are essential for helping cells survive periods of nutritional limitation. The proposed role of membrane phase separation in the TOR signaling pathway may be especially significant, as the TORC1 pathway is conserved in yeast and humans.

Moreover, our findings imply that new mechanisms of regulating the composition of yeast vacuoles may await discovery. Signaling pathways that could control phase separation in vacuole membranes in response to changes in temperature are, at best, only partially characterized. In a candidate-based screen for mutants whose membranes cannot phase separate, Toulmay and Prinz identified genes in at least three signaling pathways: the Rim system, which responds to pH, the Fab1 (also called PikFYVE) phosphatidylinositol-3-phosphate 5-kinase, which responds to osmotic gradients and other stresses, and the Slt2 (Mpk1) MAP kinase, also involved in osmotic and membrane stress responses (16). At least two of these systems are also important for cellular responses to temperature. Mutant *fab1*Δ cells exhibit severe growth defects at elevated temperature, demonstrating that Fab1 activity is indispensable for cellular thermotolerance (74). Similarly, genes encoding proteins in the Slt2 pathway are mutated under selection for thermotolerance in experimental evolution studies, and this pathway becomes constitutively active during mild heat stress (75, 76). Moreover, we previously found that both phospholipid acyl chain composition and plasma membrane membrane fluidity are regulated through the Rho1–Protein Kinase C–Slt2 signaling pathway (77).

Phase separation in the yeast vacuole, first observed half a century ago, has re-emerged as the most robust and tractable model for understanding membrane phase separation in an intact cell system. Recent results from several groups show that essential processes for domain formation include lipophagy, sterol metabolism, and probably phospholipid metabolism (16, 19, 20, 29, 55). Our results reveal an unexpectedly tight thermostatic regulation of the vacuole membrane's biophysical properties. Going forward, major challenges include dissection of the mechanisms underlying this thermostat, and tests of the downstream functional consequences of membrane phase separation. Unresolved biophysical questions include the mechanisms that facilitate or impede the merging of many small domains into a few large domains in yeast

vacuoles and the roles of transmembrane osmotic gradients and membrane tension in domain formation and structure.

MATERIALS AND METHODS

Yeast cell culture

Saccharomyces cerevisiae BY4742 (78) harboring a Vph1-GFP translational fusion was used in all experiments (*MATa his3∆1 lys2∆0 ura3∆0 leu2∆0 VPH1-GFP::HIS3*). The Vph1 fusion is one of 14 endogenous protein markers and 3 lipid probes found by Toulmay & Prinz to partition to only one of the two membrane phases of vacuole membranes in the stationary stage (16). Cultures were grown in a shaking incubator at 225 rpm using synthetic complete (SC) media containing 0.4% dextrose. For log stage experiments, cultures (1 L) were grown to an optical density @ 600 nm (OD_{600}) of 1.0 (~17 hours at 30°C).

For stationary stage experiments, cultures (10 mL) were incubated at 20°C, 25°C or 30°C. Yeast were harvested after 72 hours of growth at similar cell densities ($OD_{600} \approx 6$). Cultures at 20°C grow at a slower rate and therefore were started at a higher concentration to reach the same optical density (a proxy for growth stage) in an equivalent amount of time. We prioritized cell density because it has been shown to influence transition temperatures in cell-derived membranes (37, 38). Incubator temperature was monitored with a Fisherbrand TraceableLIVE Wi-Fi Datalogging Thermometer (0.25°C accuracy). This monitoring renders phase transition temperatures in this work more accurate than reported previously (21).

Temperature experiments

Cells were diluted for imaging in an isosmotic solution of conditioned media from the grown culture. To make conditioned media, 1 ml of culture was centrifuged at 3400×g. The supernatant was collected and centrifuged again at 3400×g rpm to remove remaining cells. To decrease refractive index mismatch (79), 200 µL of OptiPrep (60% OptiPrep Density Gradient Medium Sigma Cat # D1556) was added to 800 µL media and vortexed. Coverslips were coated with 3 µL of 1 mg/ml Concavilin-A (EPC Elastin Products Co no. C2131) in buffer [50 nM HEPES (pH 7.5, 20mM calcium acetate, 1 mM $MnSO_4$]. Immediately prior to use, the coverslips were washed with MilliQ water and dried with air. Samples of 3 µL of cells were diluted into 3 µL of conditioned media containing 12% OptiPrep and placed onto the concanavalin-A coated coverslip. Cells were sandwiched with a top coverslip and allowed to adhere to the coated coverslip for 10 min before imaging.

Images were acquired on a Nikon TE2000 frame using a Blackfly 2.3 MP Mono USB3 Vision or Teledyne Photometrics Prime 95BSI camera. Fluorophores were excited with an X-Cite 110 LED light source filtered through an IR cut filter to prevent aberrant heating of the sample from the optics. A temperature cuff (Harvard Biosciences Inc.) on the oil immersion objective (100×, 1.4 NA) was used to prevent the microscope from acting as a heat sink. Thermal grease (Omega OT-201) was used to keep the sample in thermal contact with the home-built, temperature-controlled stage (Omega Engineering). The sample temperature was measured using a thermistor probe (0.2°C accuracy, Advanced Thermoelectric). Temperature was adjusted stepwise in 2°C increments, starting at the growth temperature and increasing until domains were no longer observed. Temperature sweeps were done quickly, and only at high temperature for 3-5 min, to limit cellular thermal stress. We previously verified that yeast cells are viable following acute exposure to 50°C (21). Micrographs were taken at each 2°C interval and were used to quantify the fraction of vacuoles with domains at each temperature.

Image analysis

To preserve the fidelity of the data, image manipulation was limited to adjusting overall brightness and linear (γ=1) contrast enhancements, which was accomplished with ImageJ (http://imagej.nih.gov/ij/). To score membranes as being either uniform or phase separated, images were automatically cropped and displayed to the user using original Python code that has been made available by public license at github.com/leveillec/demixing-yeast-vacuole. The user was blind to the growth and sample temperatures for each image (Fig. 2.S5). The percent of phase separated vacuoles at each temperature was fit using

$$\% \text{ Phase Separated} = 100 * \{1 - [1 / (1 + e^{-((x-c)/d)})]\}.$$

Here, c is T_{mix}, the temperature at which the percent of vacuoles with domains is reduced by 50%, and d is the rate of the sigmoid decay.

At all temperatures, at least some vacuole membranes appear uniform, as reported by others (16, 19, 27). Data were normalized by setting the maximum percent of phase separated vacuoles to 100% for each experiment. The experiments systematically undercount vacuoles with domains because micrographs capture only one plane of the vacuole, which may not intersect with a domain. Our data also undercount vacuoles in which domains are too small to

identify; excess area in the membrane can prevent domains from merging (80). During the course of an experiment, domains can coalesce (Fig. 2.2A), rendering them easier to identify and leading to an increase in the apparent percentage of vacuoles with domains as T_{mix} is approached from low temperatures.

Vacuole isolation experiments

A 1 L culture was grown to OD_{600} = 1.0. Cells were sedimented in a swinging bucket rotor for (3200×g, 10 min, room temperature), resuspended in 0.1 M Tris (pH 9.4) and 10 mM dithiothreitol, and incubated for 10 min at 30ºC. The cells were again sedimented in a swinging-bucket rotor (3200×g) for 5 min at room temperature and then resuspended in spheroplast buffer (600 mM sorbitol, 50 mM potassium phosphate pH 7.5, and 8% growth media). Lytic enzyme (Zymolyase 20T, Seikigaku; further purified in-house by cation exchange chromatography) was added and the cells were incubated for 25 min. The spheroplasted cells were sedimented in a swinging-bucket rotor (3200×g) for 5 min at 4ºC. For hypoosmotic lysis, spheroplasts are resuspended in 15% ficoll buffer (10 mM Pipes-KOH pH 6.8, 200 mM sorbitol, and 15% w/v ficoll) and diethylaminoethyl-dextran was added to a final concentration of 0.005–0.01% w/v. Spheroplasts were incubated for 2 min on ice, then 3 min at 30ºC. The resulting spheroplast lysates were added to a SW-41 ultracentrifuge tube and overlaid with a step gradient of 8%, 4% and 0% Ficoll in PS buffer (10 mM Pipes-KOH, pH 6.8, 200 mM sorbitol). Ultracentrifugation in an SW-41Ti rotor (Beckman) at 30,000×g for 90 min at 4ºC resulted in pure vacuoles at the 4%-0% Ficoll interface.

Images of cell-free vacuoles were collected by diluting 5 µL of the isolated vacuole prep in 45 µL of low-melt 0.8% agarose prepared in PS buffer and mounted between a microscope slide and coverslip. The agarose immobilized vacuoles during imaging and prevented them from “splatting” onto the coverslip. Images were collected on an Olympus IX71 fluorescence microscope with an Andor IXON electron-multiplying charge-coupled device camera, using a 60× 1.45 NA oil immersion objective and 1.5× tube lens.

Cyclodextrin:ergosterol complex

Ergosterol was dissolved in chloroform in a glass test tube and the solute chloroform was evaporated using a gentle stream of dry N_2 to create a thin film. The film was then rehydrated in 2.5 mM methyl-β-cyclodextrin in aqueous solution. The tube was vortexed and

then sonicated in a bath sonicator for 1-3 min. The solution was incubated in a 37°C water bath overnight and used the next day.

SUPPLEMENTARY METHODS

Giant unilamellar vesicles

GUVs were prepared with 60 mol% DOPC, 20 mol% DPPC, 20 mol% ergosterol, and 0.8 mol% Texas Red DPPE and electroformed as previously described (81). Briefly, an aliquot of 0.25 mg of lipids dissolved in chloroform was spread evenly on a glass slide coated with indium-tin-oxide (ITO, Delta Technologies, Loveland CO). The slide was placed under vacuum for 30 min to evaporate the chloroform. A capacitor was created by separating two ITO-coated slides with two rectangular Teflon bars (0.3 mm thick). The gap between the bars was filled with ultrapure (18 MΩ-cm) water and all edges were sealed with vacuum grease. An AC voltage of 10 Hz and 1.5 V was applied to the capacitor for 1 hour at 60ºC. Vesicles were then extracted from the capacitor and diluted 5–10-fold in ultrapure water.

To image GUVs, several drops of vesicle stock solution were deposited between glass cover slips, and the edges were sealed with vacuum grease. This assembly was thermally coupled to a temperature-controlled stage on a Nikon Y-FL epifluorescence microscope via a layer of thermal grease. Images were captured using a 10x air objective.

Synthetic complete media recipe

Per Liter of H_2O -
1.4 g Amino Acid Mix (see below)
1.7 g Yeast Nitrogen Base (without amino acids and ammonium sulfate)
5 g of Ammonium sulfate
4 g of Glucose (0.4% glucose) or 20 g of Glucose (20% glucose)

Amino acid powder mix:

1 g Adenine	4 g Tryptophan
1 g Histidine	4 g Leucine
1 g Methionine	4 g Isoleucine
1 g Uracil	5 g Glutamic Acid
1 g Arginine	5 g Aspartic Acid
2.5 g Phenylalanine	7.5 g Valine
3 g Lysine	10 g Threonine
3 g Tyrosine	20 g Serine

SUPPLEMENTARY FIGURES

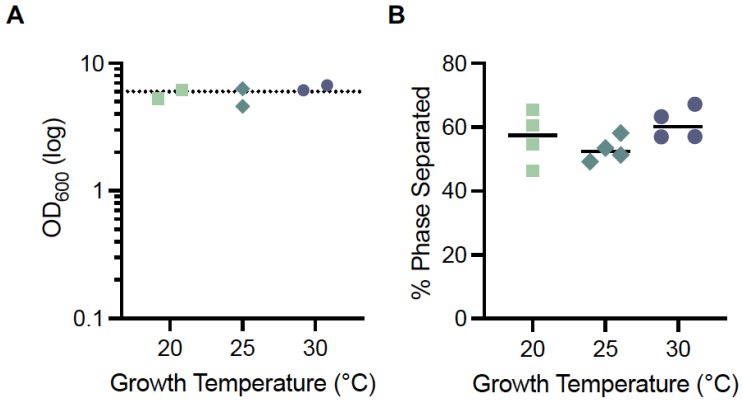

Figure 2.S1: To control for the fact that growth temperature affects growth rate in yeast cells, we **(A)** grew cells to similar optical densities (OD) after 72 hours of growth, which produced similar percentages of vacuole membranes that were phase separated (shown in panel B). Yeast grown in 0.4% glucose reach the stationary stage after ~30 h at 25°C, and after ~12 h at 30°C. To achieve similar optical densities after 72 hours, starter cultures at 25°C and 30°C were diluted back to 0.001 OD. Cultures at 20°C were diluted back to 0.1 OD. If cultures at 20°C are diluted back to 0.001 OD, after 72 hours optical densities are only ~4, and only ~20% of the vacuoles have domains, indicating that the culture is not sufficiently into the stationary stage. **(B)** Less than 100% of vacuole membranes in the stationary stage exhibit domains, as reported previously (16, 19, 27). On average, cultures grown at 30°C exhibit slightly more phase separation in their membranes than cultures grown at cooler temperatures. For each population of cells in Fig. 2.2, the maximum percent of vacuole membranes with domains was normalized to 100%.

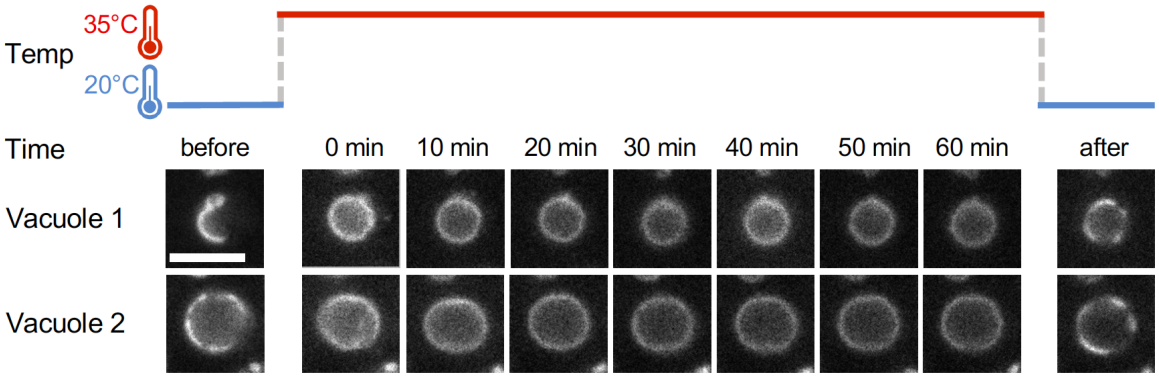

Figure 2.S2: Timescales longer than 1 hour are required for yeast to significantly remodel their vacuole membranes. Yeast were grown at a low temperature (20°C) into the stationary stage, when their vacuoles exhibited domains with a T_{mix} of 32.4 ± 1.6°C. The temperature was then raised to 35°C, just above T_{mix}. Cells were maintained at this new temperature for 1 hour. Within this time, vacuole membranes did not return to a

phase-separated state. After 1 hour, the temperature was decreased to 20°C again, and domains were observed again. Images from two representative vacuoles are shown throughout the process. Scale bar = 5 μm.

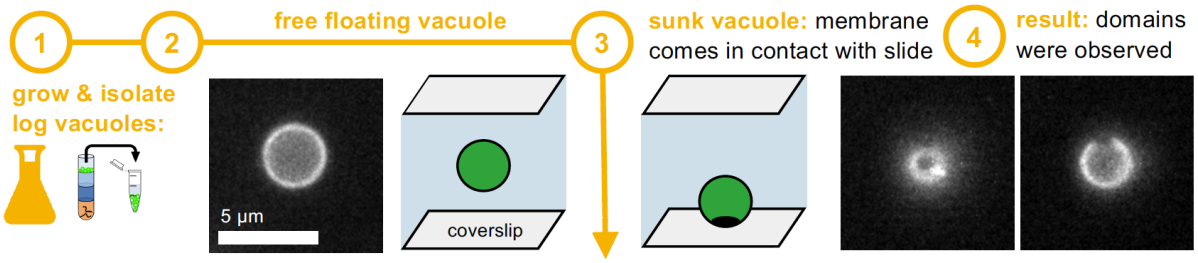

Figure 2.S3: Vacuoles isolated from the logarithmic stage of growth do not exhibit domains. When cooled to 5°C, domains were not observed in the membranes of free-floating vacuoles. However, when the vacuoles came in contact with glass slides, domains were observed. This result is consistent with results in GUVs showing that domains can nucleate when the membrane is in contact with a surface and close to a phase transition (59–61).

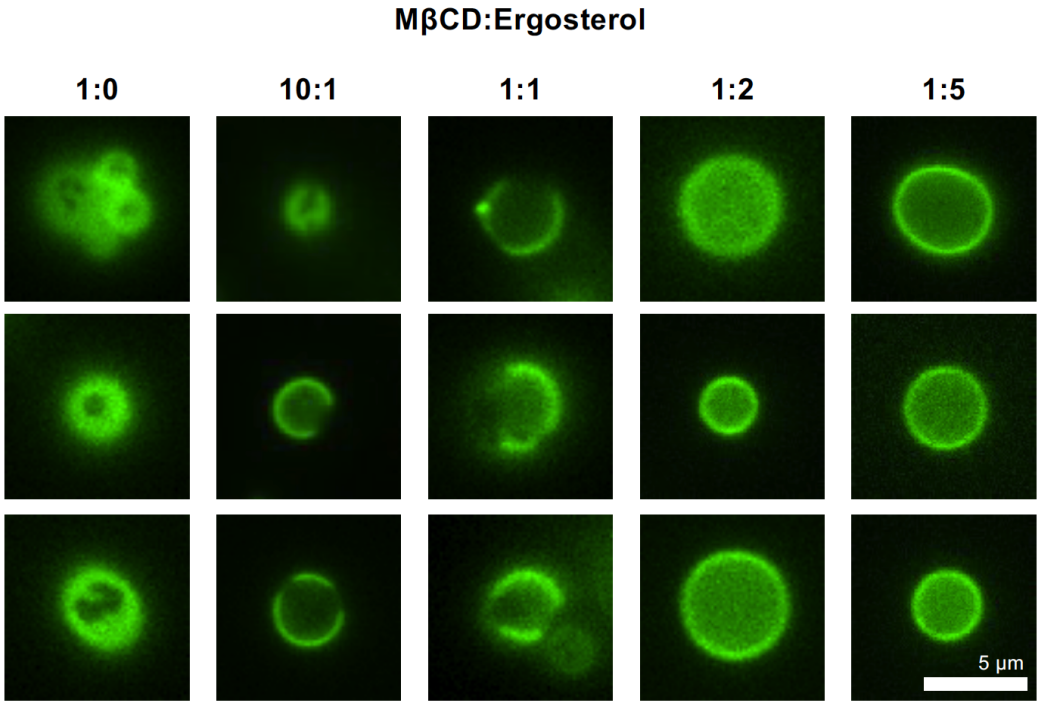

Figure 2.S4: Domains appear in membranes of vacuoles isolated from yeast in the logarithmic stage of growth when ergosterol is depleted from the membranes. Depletion is achieved by introducing MβCD and ergosterol in ratios in which MβCD is in excess (1:0 and 10:1). When vacuole membranes are supplemented with ergosterol (by introducing MβCD and ergosterol in ratios in which ergosterol is in excess (1:2 and 1:5) domains do

not appear – the membrane remains in a single phase. Introducing equimolar (1:1) MβCD and ergosterol has the same effect as depleting ergosterol from vacuoles.

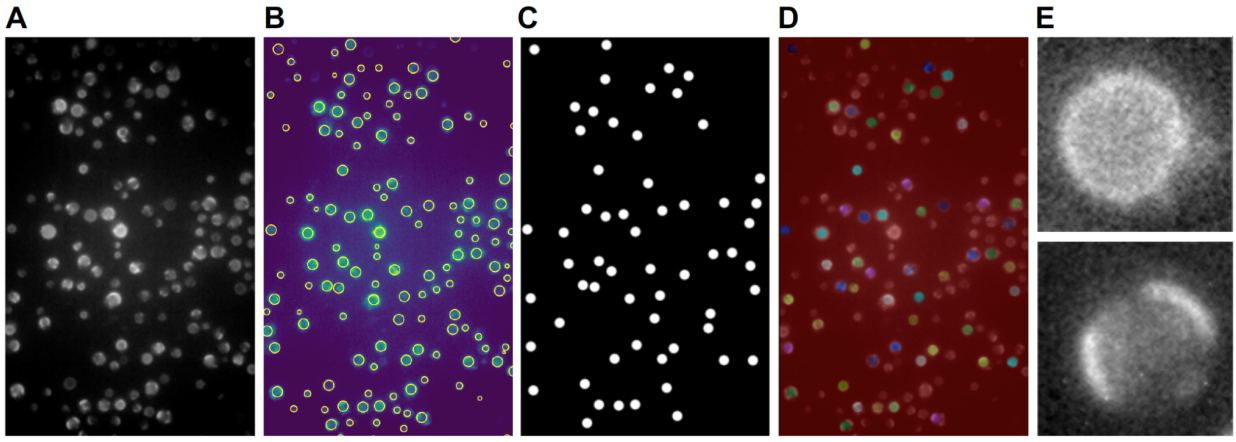

Figure 2.S5: (A) Original images contained large fields of view. At each temperature, three fields of view were analyzed. (B) Individual vacuoles were identified as bright areas in the image using a blob detection "difference of Gaussians" function (www.scikit-image.org). (C) A mask was created using the coordinates and the radius from the blob detection. Vacuoles that were too small or along the edges of the image were discarded. (D) The vacuoles that remained were identified and individually cropped. (E) Each cropped vacuole was displayed and scored by the user as mixed (top) or demixed (bottom). The scorer was blind to the growth and sample temperatures for each cropped image. The scorer was also unable to see the whole field of view, so the temperature could not be easily deduced. Original Python scripts and the images above are available by public license at github.com/leveillec/demixing-yeast-vacuole.

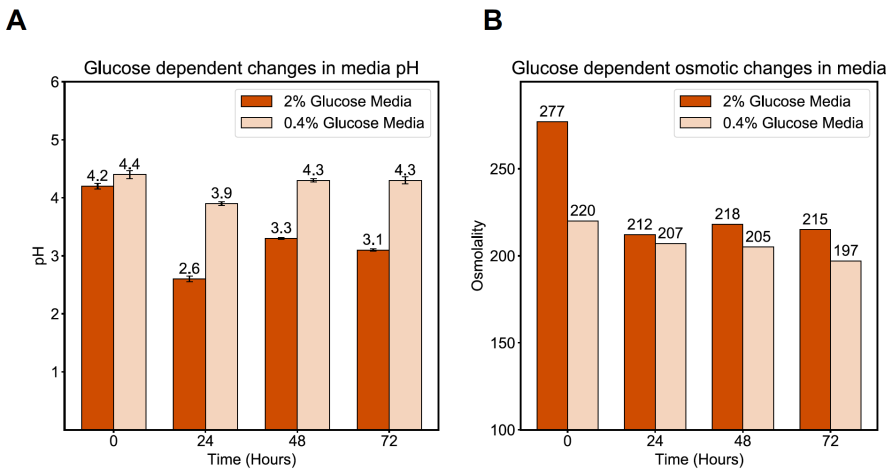

Figure 2.S6: Media conditions are important to control because phase separation in vacuole membranes can occur in response to glucose depletion, acid stress, and osmotic shifts (16). (A) To minimize confounding effects from different stressors, we used SC

media with 0.4% glucose, as opposed to 2% glucose because the pH of the media does not vary significantly through time when yeast are grown in 0.4% glucose. In contrast, when yeast are in media with 2% glucose, a large decrease in pH is observed as the cell metabolizes glucose into toxic species, including acetic acid (82). Error bars show the standard deviation of 3 measurements of the same sample. (B) Another reason that SC media with 0.4% glucose is preferable is that it does not result in a large osmotic shift during growth, whereas 2% glucose does. This experiment was performed once.

Composition	Measured T_{mix}	Change	Membrane ergosterol
GUV: 60/20/20 - DOPC/DPPC/Erg	26.2 ± 0.3°C	–	Initial conditions
10:1 MβCD:ergosterol added to GUVs	29.4 ± 0.4°C	Increase in T_{mix}	Membrane ergosterol depleted
1:1 MβCD:ergosterol added to GUVs	26.2 ± 0.2°C	No change in T_{mix}	Ergosterol was added and removed at the same rate
1:2 MβCD:ergosterol added to GUVs	21.8 ± 0.2°C	Decrease in T_{mix}	Membrane ergosterol supplemented

Table 2.S1: Depleting ergosterol from giant unilamellar vesicles (GUVs) increases T_{mix}; supplementing ergosterol decreases T_{mix}. GUVs were made of 60 mole % dioleoyl-phosphatidylcholine (DOPC), 20% dipalmitoylphosphatidylcholine (DPPC), and 20% ergosterol. Depletion was achieved by introducing MβCD and ergosterol at a ratio in which MβCD is in excess (10:1). This level of depletion of ergosterol increased T_{mix} by ~3°C. Supplementation was achieved by introducing MβCD and ergosterol at a ratio in which ergosterol is in excess (1:2). This level of supplementation decreased T_{mix} by ~4°C.

CHAPTER 3

Lipidomics of the yeast vacuole

The research in this chapter was conducted in collaboration with J. Reinhard, C.E. Cornell, R. Ernst, A.J. Merz, and S.L. Keller.

INTRODUCTION

During normal growth, cells undergo enormous changes to adapt to their environment. For example, when yeast (*Saccharomyces cerevisiae*) become nutrient limited, they shift from exponential (log stage) growth to a slower (stationary stage) growth. This shift is accompanied by striking changes in vacuoles, the lysosomal organelle of yeast. The vacuoles merge so that most cells contain only one large vacuole, and their outermost membranes undergo liquid-liquid phase separation (Fig. 3.1) (21). This phase transition induces micron-scale membrane domains that are enriched in particular lipids and proteins (15, 16, 19, 28). This transition can be reversed by raising the temperature of the yeast to about 15°C above their growth temperature (83). Recent studies suggest that phase-separated domains regulate the cell's metabolic response to nutrient limitation through the TORC1 pathway, which regulates protein synthesis, autophagy, docking of lipid droplets, and other processes (16–20).

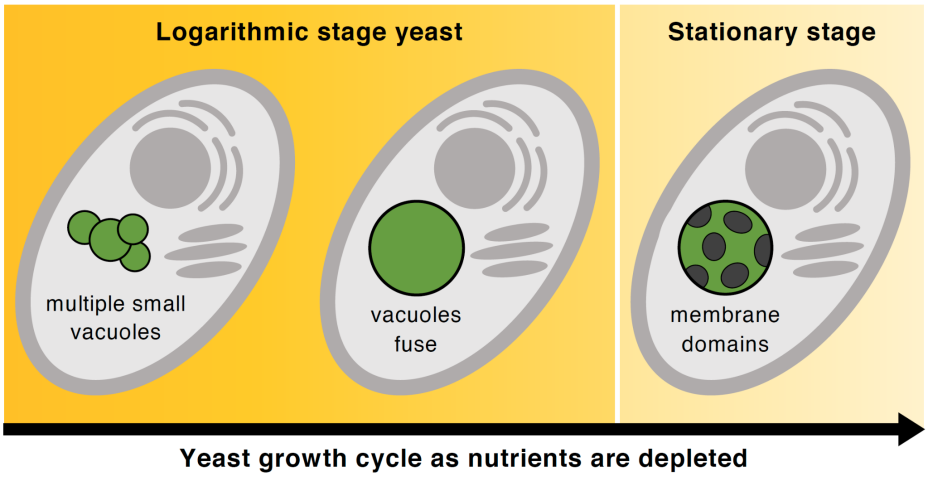

Figure 3.1: In nutrient-rich media, yeast grow exponentially. In this "logarithmic stage", each cell contains multiple small vacuoles, the lysosomal organelle of yeast. As nutrients become limited, the vacuoles fuse, and yeast enter the stationary stage. In this stage, the vacuole membrane phase separates into two coexisting liquid phases.

An outstanding question in the field has been how yeast control phase separation in their vacuole membranes? Specifically, what changes do yeast make to the lipidome of their vacuole membranes as they enter the stationary stage of growth? We expect the lipidome to change because the few mutations that perturb phase separation of the vacuole involve lipid trafficking and metabolism (16, 19, 29).

Previous attempts to measure changes in vacuole lipidomes were limited by the technical challenge of isolating vacuole membranes from the membranes of other organelles. This challenge is formidable because it is known that vacuole membranes are in contact with other membranes, such as the nuclear envelope, which can co-purify with vacuoles (84). Nevertheless, we know that changes in the vacuole lipidome from the log stage to the stationary-stage must be significant because large decreases in temperature (from 30°C to 5°C) are not sufficient to induce log stage vacuole membranes to phase separate, whereas stationary-stage vacuole membranes phase separate at several growth temperatures (83). What are these changes in the lipidome? In the past, researchers have focused on ergosterol, the predominant sterol in yeast. Phase separation in isolated vacuoles is reversed through changes in ergosterol levels (16, 55, 83). Zisner et al. used a coarse isolation procedure to enrich vacuoles and found that vacuoles contain ~15% ergosterol in the logarithmic stage of growth (63). Progress toward evaluating the full lipidome was also made by Klose et al., who measured changes in the whole cell lipidome through the growth cycle. They found that ergosterol in the log stage was ~14% and was reduced to ~10% in the stationary stage (71). However, it remained unclear how much of this change could be ascribed to the vacuole membrane alone.

Here, we employ immunoaffinity techniques to efficiently separate membranes of vacuoles from those of other organelles (85). A key step in immunoisolation is to endogenously label a protein that resides only in the membrane of interest. To ensure equal immunoisolation efficiencies in the log and stationary stage growth, we used membrane protein Mam3 as our bait, which isolates both membranes at good yields. By coupling immunoisolation techniques with lipidomics, we build a detailed map of how the lipid profile of the vacuole membrane changes as yeast shift from logarithmic growth to the stationary stage. We put our lipidomic data into context by leveraging existing data on the physical properties of lipids to infer how changes in the lipidome of an organelle may enable membrane phase separation in living cells.

RESULTS

Mam3 is a robust bait protein for immunoisolation of vacuole membranes

We identified several membrane proteins as candidate "bait proteins" for immunoisolation of vacuoles in *both* the log stage and the stationary stage of growth. For our application, a robust bait protein (1) must have its c-terminus available in the cytosol, (2) contains an intramembrane domain anchoring it to the membrane, (3) partitions to only the vacuole, and (4) is expressed at high levels in both the log and stationary stage. Bait proteins are crucial because they provide a high level of organelle selectivity that is not available by standard flotation methods (Fig. 3.2A,1-3). In detail, bait proteins are connected to a molecular "bait" (the construct myc-3c-3xFLAG) that links the protein (and the membrane in which it resides) to beads coated with anti-FLAG antibodies for isolation. Isolated membranes are subsequently cleaved from the beads (using GST-3c) and analyzed by lipidomics (Fig. 3.2B).

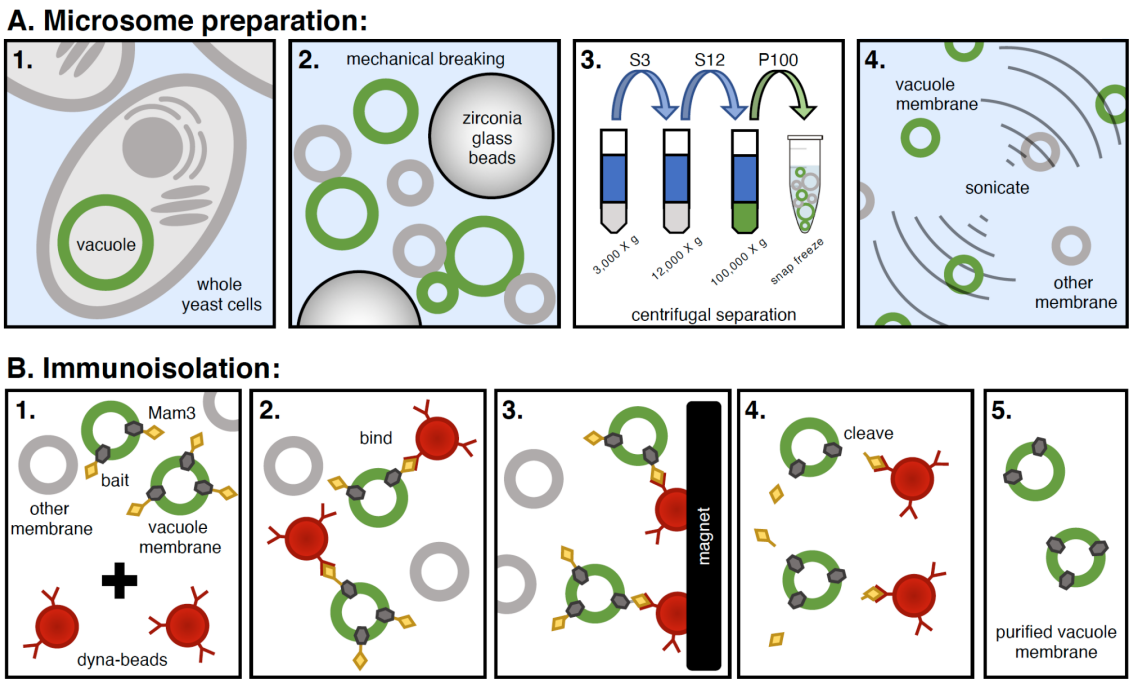

Figure 3.2: A. (1) Yeast cells are grown to either the log or stationary stage. **(2)** Cells are mechanically fragmented with zirconia glass beads using a fast-prep shaker. **(3)** Cellular debris and other organelle membranes are separated from the vacuole membranes using a series of centrifugation steps. The fraction of the sample containing vacuole membranes (either the supernatant, S, or the pellet, P, was retained. **(4)** Sonication breaks contact sites between vacuole membranes and other organelles and produces smaller microsomes for immunoisolation. Items are not drawn to scale. **B. (1)** Top: The microsome solution is enriched in vacuole membranes, which are labeled with a bait tag (myc-3c-3xFLAG) attached to Mam3 proteins. Bottom: Microsomes are mixed with magnetic dyna-beads coated with an antibody to the bait protein (anti-FLAG). **(2)** The

dyna-beads bind to vacuole membranes, and not to other membranes. **(3)** The dyna-beads are immobilized by a magnet. The solution was serially washed to remove unbound membranes. **(4)** Vacuole membranes are cleaved from the beads with GST-3C protease. **(5)** Removal of the dyna-beads leaves purified vacuole membranes for lipidomics.

An obvious candidate was Vph1, which has high expression levels in the log stage of growth (16, 86). It has been extensively used for visualizing vacuole domains (16, 19, 21, 28, 29, 83), and was previously used by us (Fig. 3.S6) for immunoisolation in that stage. However, in the stationary stage, the Vph1-bait construct resulted in an insufficient yield of membranes (Fig. 3.S1).

In contrast, Mam3 proved to be an excellent bait protein. We confirmed previous reports that Mam3 partitions to the vacuole membrane (87) by showing that Mam3 colocalizes with FM4-64, a styryl dye that selectively stains vacuole membranes (Fig. 3.S2). In the log stage, when vacuoles do not exhibit domains, Mam3 distributes uniformly on the vacuole membrane (Fig. 3.3A and Fig. 3.S2). When the cell enters the stationary stage, Mam3 partitions to only one of the two membrane phases (Fig. 3.3A,B). Specifically, Mam3 partitions to the same phase as Vph1, which Toulmay & Prinz identified as a liquid disordered (Ld) phase (Fig. 3B and 3.S3) (16). Abundance of Mam3 remains high in both the log and stationary stages (Fig. 3.3C).

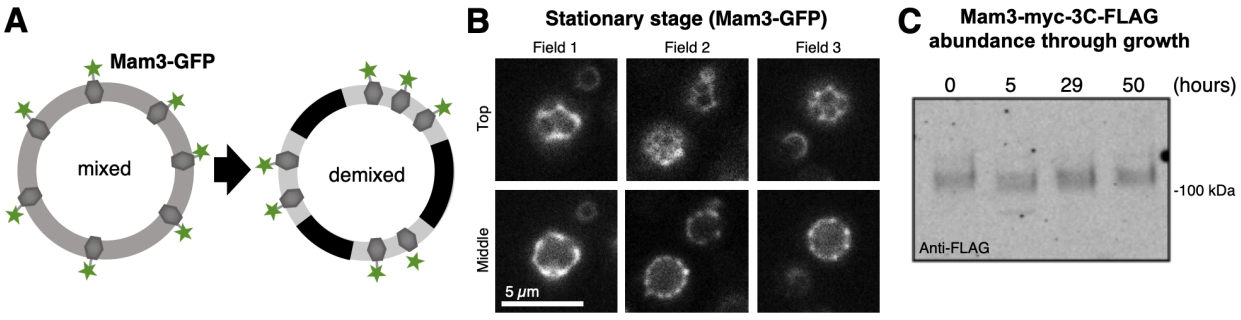

Figure 3.3: (A) In the log stage of growth, lipids and proteins appear uniformly distributed in vacuole membranes of yeast. We endogenously label Mam3, a protein in vacuole membranes, with a bait tag for immunoisolation or with GFP for fluorescence microscopy. **(B)** Fluorescence micrographs of yeast in vivo showing that in the stationary stage (after 48 hours of growth), the vacuole membrane phase separates into two liquid phases. Mam3 partitions into only one of these phases. Micrographs were taken at room temperature at both the top ("Top") and the midplane ("Middle") of vacuoles for each field of view. Wider, representative fields of view are shown in Fig. 3.S4, and corresponding images for Vph1 are in Fig. 3.S3. (C) Fluorescent western blot showing the expression levels for Mam3 measured through the growth cycle at 0, 5, 29, and 50 hours. Mam3 was

visualized using the fluorescently labeled antibody anti-FLAG which binds to the endogenous tag myc-3c-3xFLAG attached to Mam3. Bands in the gel representing Mam3 elute close to 100 kDa and are relatively equal in density and size in the log and stationary stages.

Low contamination by non-vacuolar proteins and lipids

A challenge in subcellular membrane isolation is that most organelles are in physical contact with other organelles. We couple our immunoisolation approach with a sonication step that breaks contact sites and produces smaller microsomes (Fig. 3.2A, 4). We benchmark the purity of isolated vacuole membranes by verifying that protein markers for other organelles are depleted from post-immunoisolation fractions and that vacuole markers are enriched. For example, Dpm1, which localizes to the endoplasmic reticulum, and Por1, which localizes to the mitochondrial outer membrane, are initially present after sonication of microsomes ("load" column in, Fig. 3.4) and are removed following immunoisolation ("eluate" column in Fig. 3.4). In contrast, Vac8 and Vph1, which localize to the vacuole, are appropriately enriched in the immunoisolation eluate (Fig. 3.4). FLAG, part of the tag attached to Mam3, is not present in the final isolate fraction (pellet (10x)) because it was cleaved off to release the vacuole membrane from the dyna-beads.

In previous work by other groups, vacuole membranes were isolated from the P12 fraction because of a large amount of vacuole membrane pellets at 12,000 x g. Here, we chose to isolate membranes from the 12,000 x g supernatant fraction. While there is vacuole marker present in the pellet, our results show a significant amount of vacuole present in the supernatant. We were willing to sacrifice some yield to increase specificity because less contaminant membranes float in the supernatant (Fig. 3.4).

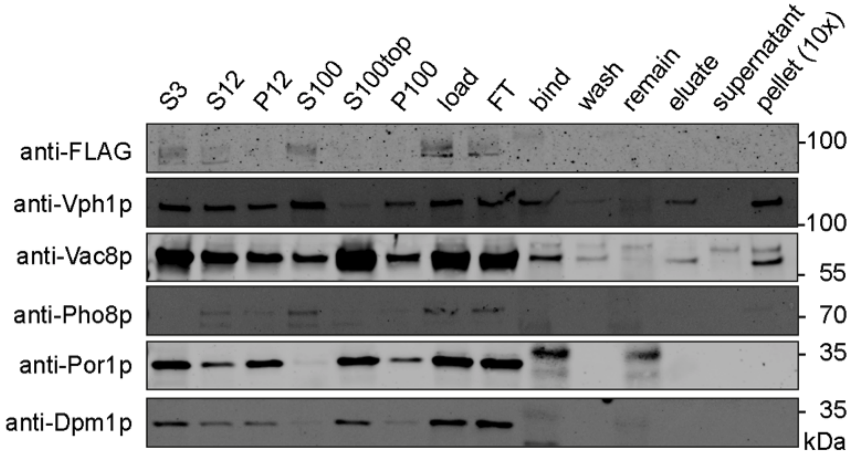

Figure 3.4: Labels at the top of the bands denote steps in the immunoisolation process. “S” denotes supernatant, “P” denotes pellet, and the number denotes thousands of g’s of centrifugal acceleration. For example, S100 is the supernatant after centrifuging at 100,000g. Prior to immunoisolation, proteins that reside in membranes of the endoplasmic reticulum (Dpm1) and mitochondria (Por1) are present in microsome preparations of yeast (“load” column). Bands representing anti-FLAG bait proteins (Mam3) and vacuole markers (Vph1, Pho8, and Vac8) show excellent binding to antibody-coated dyna beads (“bind” column). Immunoisolation removes membranes of the endoplasmic reticulum and mitochondria (seen by an absence of Dpm1 and Por1 in the “eluate” column) and retains only vacuole membranes for lipidomics (seen by bands for Vac8 and Vph1 in the “eluate” and pellet (10x) columns).

We also evaluate the purity of isolated vacuole membranes by assessing contamination by triacylglycerols (TAG) and ergosterol esters. Isolation of pure vacuole membranes is particularly challenging in the stationary stage, when lipid droplets are produced in high numbers and are in intimate contact with vacuole membranes (19, 29, 88). The lumens of vacuoles become filled with storage lipids from lipid droplets (TAG and ergosterol esters) (19). These storage lipids have low solubility (< 3% for TAG) in phospholipid membranes, and even lower solubility when the membranes contain sterols (89, 90).

We find that only ~2.5% of all lipids isolated with log stage vacuoles are TAG, and < 1% are EE. For stationary-stage lipids, we find ~13% TAG and < 1% ergosterol esters (Fig. 3.S5). These contamination levels are significantly lower than Zinser et al. who found that ~4% (in contrast to our result of 0.3% ergosterol esters) of all phospholipids, sterols, and steryl esters were ergosterol esters in the logarithmic stage of growth. In comparison, in whole cells in the stationary stage, TAG = > 30% of all lipids (Fig. 3.S5). Because the solubility of storage lipids in membranes is so low in phospholipid bilayers and because they likely originate from lipid droplets, we excluded them from our subsequent lipidomic analysis.

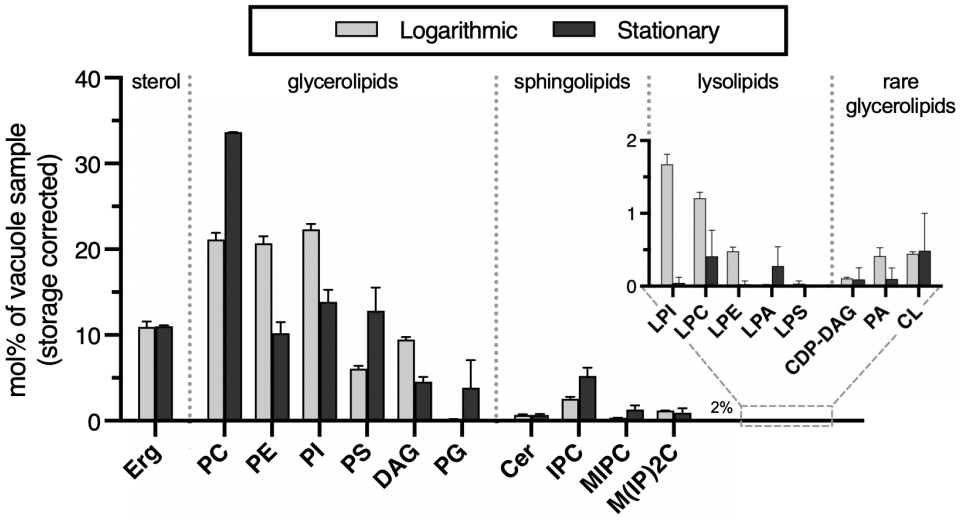

Figure 3.5: Dramatic changes occur in the abundance of several types of lipids in yeast vacuoles in the logarithmic stage vs. the stationary stage. Among the common glycerolipids, increases of ~50% or more are observed in PC-lipids, PS-lipids, and PG-lipids (to unusually high levels), whereas concomitant decreases are observed in DAG, PI-lipids, and PE-lipids. Among less prevalent lipids, sphingolipids tend to increase and lysolipids tend to decrease. Data exclude the "storage lipids" found in the lumens of lipid droplets; full data sets are in Fig. 3.S5. Acronyms of all lipids are listed in Table 3.S1.

Logarithmic stage lipidomes have high levels of PC, PE, and PI lipids

We quantified the lipidome for ~520 individual lipid species, in 22 lipid classes. Lipidomes of log stage vacuole membranes immunoisolated with Mam3 are in excellent agreement with those we previously isolated with Vph1 (Fig. 3.S6). In general, vacuole membranes are abundant in the common lipid classes: PC, PE, and PI (Fig. 3.5). Compared to whole-cell lipodomes of yeast, the vacuole is distinguished by a fraction of PA lipids that is ~2x lower, whereas the fraction of DAG and PS lipids is ~2x higher than the whole cell data from Klose et al. 2012 (71). Error bars in Fig. 3.5 show low standard deviations of lipidomes collected on different days.

A central question is why log stage vacuole membranes do not phase separate, whereas stationary-stage membranes do. Membrane phase separation is often associated with sterol content. In yeast, the major sterol is ergosterol. Ergosterol levels in the log stage vacuoles (and whole cell lipidomes) are high enough to achieve phase separation in model ternary membranes. Therefore, it is reasonable to expect that phase separation in stationary stage vacuole membranes is driven by changes in the carbon chains of lipids, specifically in their length and unsaturation, as we will explore in the next section.

Dramatic changes occur from the log stage to the stationary stage

In Fig. 3.5, the starkest change in the vacuole's lipidome is the jump in the fraction of PC lipids. This jump is particularly notable because it does not occur on a whole-cell level and because PCs are a large fraction of the vacuole's lipids (71). What could the vacuole membrane achieve through this jump in PC content that other membranes in yeast do not? Additional increases in vacuole lipids that are not reflected in the whole-cell lipidome include jumps in PS, PG and IPC (a sphingolipid), all to unusually high levels. In contrast, decreases in PE, PI, and DAG lipids reflect decreases in the whole-cell lipidome. PA lipids are surprisingly scant in both log and stationary-stage vacuoles.

Sterol levels are similar in log and stationary stages

We find that the molar fraction of ergosterol is similar in vacuoles during logarithmic and stationary stages (Fig. 3.5). It is known that sterols are key molecules required for liquid-liquid phase separation in model membrane systems (4, 9, 51–54). While ergosterol levels do not change, there is ample sterol (~10%) for phase separation of the membrane to occur in the stationary stage. It is also known that other physical properties of lipids such as their saturation and length are important for phase separation in established model systems (4, 9, 51–54). These results suggested that other lipids and their structures may influence micron scale phase separation in a living cell, especially when sterol levels are held constant.

Next, we analyze the melting temperatures of lipid components to determine their contribution to the overall transition temperature and phase separation of the vacuole membrane.

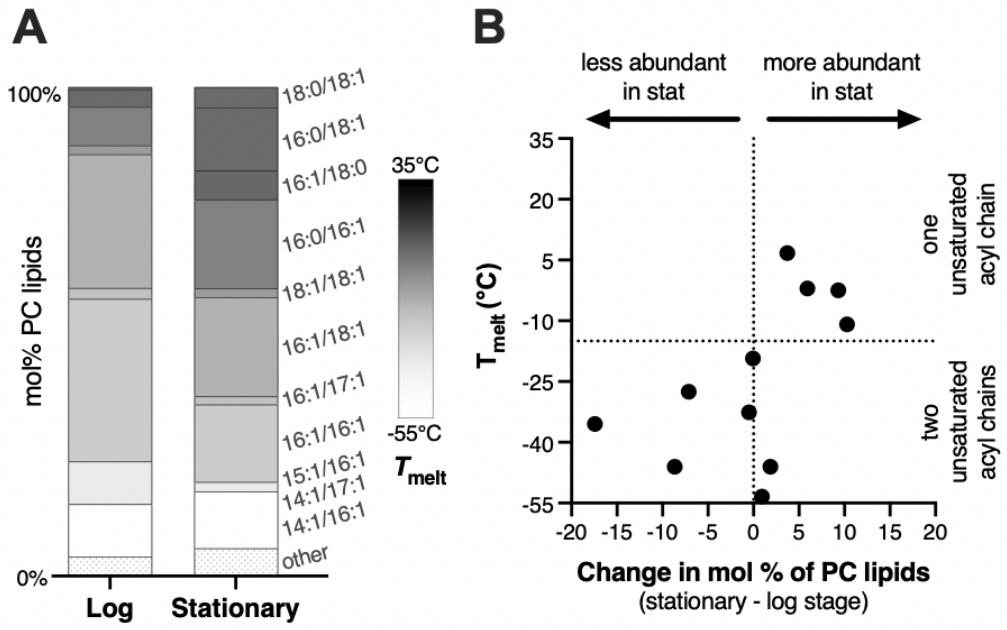

Figure 6: (A) Melting temperatures are higher for vacuole PC-lipids in the stationary stage compared to the log stage. Lipids contributing to less than 1 mol% are categorized as "other". (B) The change in mol% of lipids shows that the melting temperatures are higher for vacuole PC-lipids in the stationary stage compared to the log stage, reflected by an increase in saturation of the acyl chains. Each point represents a different PC-lipid species shown in Panel A.

PC-lipids shift to higher melting temperatures in the stationary stage

PC-lipids are abundant. Like PE and PI, this lipid class constitutes a large fraction (20-25%) of all lipids in log stage vacuole membranes. In the stationary stage, the proportion of PC lipids shoots up to about ⅓ of vacuolar lipids, the largest increase of any lipid type. Therefore, the onset of phase-separation of vacuole membranes is likely to be linked to changes in the fraction of PC lipids and in the details of their acyl chains. Changes in acyl chains lead to changes in lipid T_{melt} values. Here, T_{melt} values of PC lipids were found in the literature (91–95) or estimated (Tables 3.S2,3 and Fig. 3.S7).

Our results show that PC-lipids undergo significant acyl chain remodeling from the log stage to the stationary stage. We find that the melting temperatures are higher for vacuole PC-lipids in the stationary stage compared to the log stage (Fig. 3.6). This can be visualized in Fig. 3.6A, by a decrease in the mol% of lipids with light bands representing low melting temperatures and an increase in the mol% of lipids with dark bands representing high melting temperatures. Indeed, there is a direct trend with the number of saturated acyl chains and their

abundance in the log and stationary stage. PC lipids with two unsaturated acyl chains (low melting temperatures) are less abundant in the stationary stage. PC's with one unsaturated acyl chain (high melting temperature lipids) are more abundant in the stationary stage (Fig. 3.6B). The weighted average of T_{melt} is -31°C in the log stage and -21°C in the stationary stage, showing that PC lipids shift to higher melting temperatures in the stationary stage.

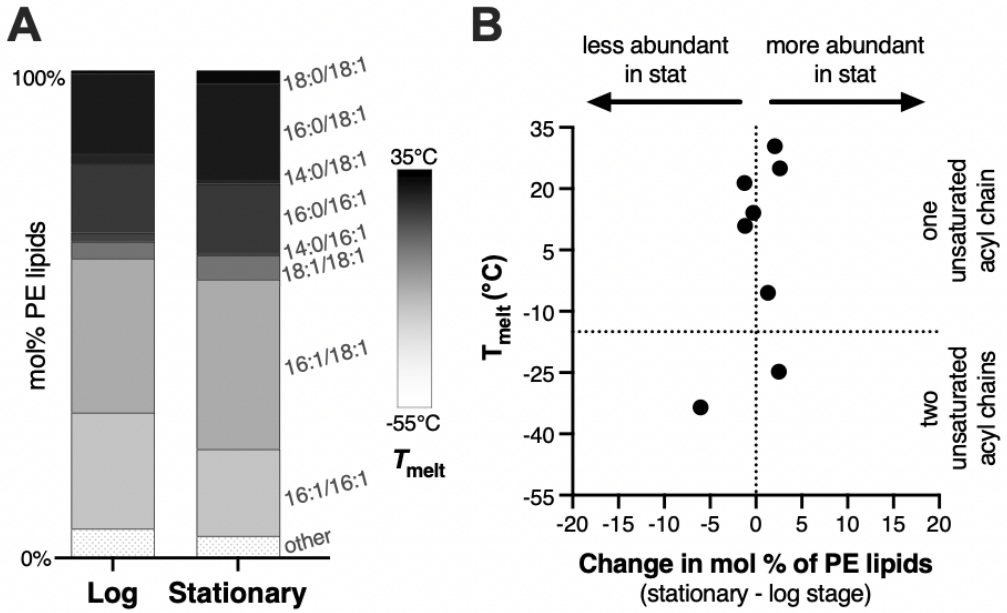

Figure 3.7: (A) Melting temperatures are similar for vacuole PE-lipids in the stationary stage compared to the log stage. Lipids contributing to less than 1 mol% are categorized as “other”. (B) Each point represents the different PE-lipids species. The change in mol% of lipids shows that the melting temperatures are the same for vacuole PE-lipids in the stationary stage compared to the log stage, reflected by a slight increase and slight decrease of low and high melting temperature lipids.

PE lipids have similar melting temperatures in log and stationary stage

Next, we analyzed the acyl chains of the PE lipids because they have the largest decrease (~10%) of any lipid in the lipidome. Many of the T_{melt} values for PE lipids were available in the literature (92, 96–98) or easily estimated (Tables 3.S2,3 and Fig. 3.S8), unlike PI and PS lipids.

While the overall amount of PE lipids was greatly reduced, we find that acyl chains of PE lipids were not heavily remodeled. Therefore, the melting temperatures of the PE lipids do not change very much: the weighted average of the T_{melt} for PE lipids is -7°C and -5°C in the log and stationary stages, respectively. We find that the melting temperatures of PE lipids are generally

high as indicated by the darker shades in the bar graph (Fig. 3.7A) and the majority of the lipid data points with one saturated acyl chain (Fig. 3.7B). Especially when compared with the PC lipid profile which are much lower, with a greater number of lipids with one unsaturation (Fig. 3.7A&B).

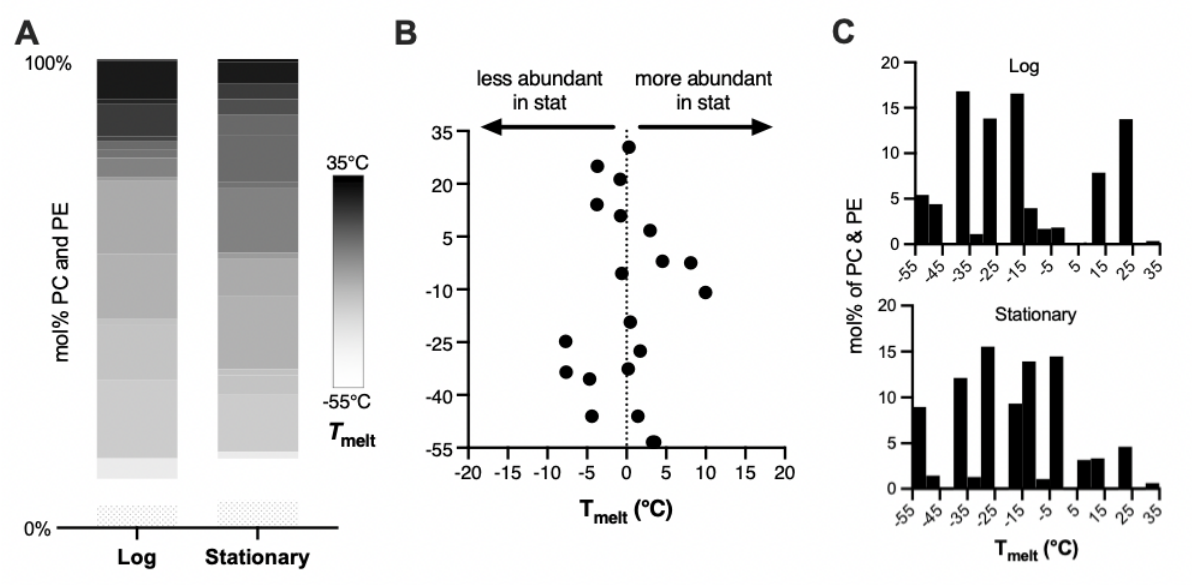

Figure 3.8: (A) Cumulative effect of the PC and PE lipids, weighted to account for the increase in the fraction of PC from log to stationary and the decrease in the fraction of PE from log to stationary. (B) Each point represents the different PC or PE-lipids species. The change in mol% of lipids shows that the melting temperatures decrease the most at low melting temperatures and slightly at high melting temperatures. Lipids at intermediate to high melting temperatures are increasing in the stationary stage. (C) Histogram of the cumulative effect of the PC and PE lipids in the log and stationary stages of growth.

PC and PE lipids cumulative effect on overall melting temperature

Unfortunately, T_{melt} values have only been measured for a small fraction of lipid types. This paucity is driven by the fact that synthetic, pure lipids have been commercially available for a limited number of years and that although some lipids types are relatively inexpensive, the expense of others makes T_{melt} measurements (which require a lot of sample) cost prohibitive.

We established that changes in PC lipids have a large effect in T_{melt} (Fig. 3.6), and that there is not a big change in PE lipid melting temperatures (Fig. 3.7). Given that the fraction of PC lipids are increasing and PE lipids are decreasing, how does that change the overall melting temperature of the membrane? The combined effects of PC and PE lipids result in nuanced changes (Fig. 3.8). It appears that lipids at the extreme melting temperatures (very high and very low) are decreasing (Fig. 3.8A,B). Whereas the lipids at intermediate to high melting

temperatures are increasing in the stationary stage (Fig. 8A,B). This cumulative PC and PE data result in little change in the weighted average of T_{melt} which is -19°C in the log stage and -17°C in the stationary. Overall there is only a slight increase in T_{melt}. Another way to visualize the summed PC and PE data is through histograms (Fig. 3.8C).

Together, PC and PE lipids only make up ~50% of the overall lipids in the stationary stage. Therefore, this research provides added impetus for the importance of the community measuring T_{melt} values for more types of lipids.

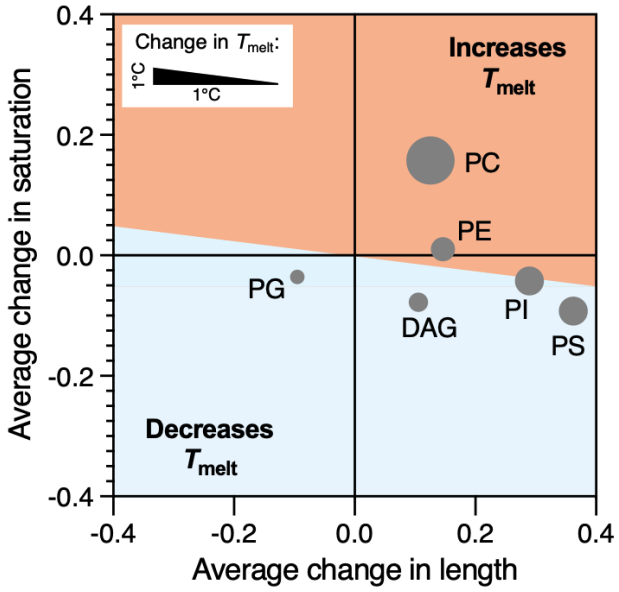

Figure 3.9: Each point represents a different glycerolipid species. The size of each point roughly represents the relative abundance of that lipid class in the stationary stage. Changes in acyl chain saturation have large effects on T_{melt} compared to changes in length. Lipids located above the diagonal increase T_{melt}. Along the diagonal line, T_{melt} does not change, and below T_{melt} decreases.

T_{melt} trends for all glycerolipids

Changes in acyl chain saturation and changes in acyl chain length affect the melting temperature in predictable ways: increasing saturation and increasing chain length will increase T_{melt}. Using this information, we can determine how all the abundant glycerolipids in the membrane effect T_{melt}.

Using known T_{melt} trends based on PC lipids (91, 92), we estimated how the overall melting temperature of the vacuole membrane is changing (Fig. 3.9 legend). The average chain

length for vacuole glycerolipid lipids ranges from 16-17 carbons. An increase in length for a saturated PC lipid from 16 to 17 carbons results in a ~5°C increase in T_{melt}. Therefore a change in 0.2 length (⅕ carbons) is ~1°C change in T_{melt}. Most lipids in the vacuole membrane have either 1 or 2 acyl chains with an unsaturation. For an average chain length between 16-18 carbons long to go from 1 to 2 unsaturated acyl chains results in a change in T_{melt} of ~40°C. Therefore a 0.025 change in saturation degree equates to a ~1°C change in T_{melt}.

As previously shown, changes in PC lipids result in a huge increase in melting temperature while PE only increases a small amount (Fig. 3.9). PI lipids, which decrease from the log to the stationary stage (Fig. 3.9), lie directly on the line where the change in saturation and the change in length have negating effects on each other, resulting in no change of the T_{melt}. Meanwhile, PS lipids, which increase in abundance (Fig. 3.5) are slightly decreasing in T_{melt} from the log to the stationary stage (Fig. 3.9). PG and DAG also decrease in T_{melt} (Fig. 3.9), however, they are much less abundant, each individually making up ~4% of the stationary stage lipidome (Fig. 3.3). In addition, from the log to the stationary stage, the percent of glycerolipids with no unsaturated acyl decreases by 5%. Concurrently glycerolipids with one unsaturated acyl chain increase by ~7% in the stationary stage increasing T_{melt} (Fig. 3.S9).

DISCUSSION

Our results provide new information about the lipidome of yeast vacuole membranes in the stationary stage, particularly in comparison to yeast in the logarithmic stage. In previous work (63, 99 and Fig. 3.S6) lipidomics had been conducted on yeast grown into the mid-log and late-log stages, not in the stationary stage.

Immunoisolation

Previous lipidomics studies on vacuoles used traditional purification methods presented in Uchida et al., where yeast cells are first converted into spheroplasts, followed by several isolation steps using flotation and density gradients (63, 99, 100) [see Table 3.S4 for comparisons]. While these methods represent an important advance in the field, membranes of other organelles (which are attached to vacuole membranes through organelle-organelle contact sites) typically contaminate membranes that are isolated in this way. The method that we use to isolate vacuole membranes is superior because it breaks those contact sites.

Moreover, the bait protein used in immunoisolation provides selectivity that is unattainable in flotation methods. The bait tag can be added to any protein in the yeast genome using conventional methods in molecular biology. However, this procedure can be laborious. Excitingly, Prof. Maya Schuldiner at the Weizmann Institute of Science has generated a genome-wide library of bait proteins; each strain has a single protein equipped with the appropriate tag at the C-terminus for immunoisolation from every possible organelle. The library will be included in our upcoming accompanying manuscript by Reinhard et al. 2022, making this isolation technique widely accessible for future organelle isolation experiments.

Representative sampling of the stationary vacuole lipidome

In the stationary stage, Mam3 preferentially partitions to the L_d phase (Fig. 3.2A,B). Breaking down vacuoles into microsomes provides a chance for selective loss of vacuole membranes without Mam3. Therefore, is it possible that our results over-samples the L_d phase.

The possibility that Mam3 over-samples the L_d phase affects the interpretation of the results presented here. For example, we found that the mole percent of ergosterol is roughly constant from the logarithmic to the stationary stage (Fig. 3.3). This result was surprising because several experiments have led to hypotheses that sterols may regulate the formation and maintenance of membrane domains in yeast. These experiments mutated genes involved in the synthesis, transport, or metabolism of sterols (16–19, 29, 55), perturbed lipid droplets (rich in sterol esters) (19, 20), and directly manipulated sterols in isolated vacuoles (16, 83). Sterol fraction is equally important in model membranes; changes in sterol fraction can drive model membranes across a miscibility phase boundary (6, 9, 51, 68). Typically, the mole fraction of sterols in L_d phases is lower than that in L_o phases (101). If our results under-sample the L_o phase in yeast vacuoles, then it is likely that overall ergosterol levels *do* increase in the stationary stage.

Conversely, if Mam3 does not over-sample the L_d phase, then our data in Fig. 3.5 accurately captures the lipidome of stationary-stage vacuole membranes. It would not be surprising to find that Mam3 samples both phases (L_o and L_d) given that the stationary-stage membrane immunoisolated with Mam3 contains a relatively high fraction (~10%) of ergosterol (Fig. 3.5), and ergosterol partitions to the L_o phase, as previously shown by filipin staining (16).

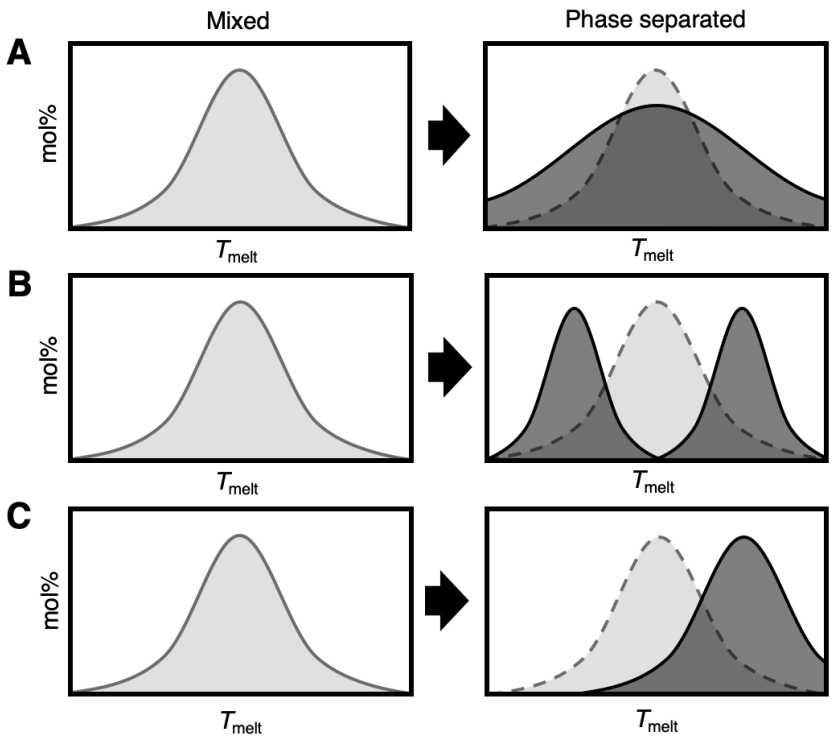

Figure 3.10: Possible lipidomic signatures of phase separation and of oversampling of one phase. **Left Columns:** In the logarithmic stage, lipids in vacuole membranes mix in one uniform phase. Those lipids have a distribution of T_{melt} values. **Right Columns:** In the stationary stage, lipids phase separate. **(A)** One possible signature of a lipidome that phase separates could be a broadening of the distribution. Lipids with very high T_{melt} values would be likely found in the L_o phase and lipids with very low T_{melt} values would be likely found in the L_d phase. **(B)** Less likely (but possible) is that the distribution would bifurcate into two distributions, one with high T_{melt} values and one with low high T_{melt} values. **(B)** If our results over-sample the L_d phase, then we expect that the distribution of lipids would shift from the overall population in the log stage to a subpopulation centered at a higher T_{melt}.

Lipidomic signatures of phase separation

We did not observe a clear lipidomic signature of phase separation in stationary-stage vacuole membranes (nor did we observe a signature of mixing in log stage membranes) (Fig. 3.8C). In model membranes, membranes that contain only one phospholipid and a sterol, no micron-scale phase separation is observed (4). Therefore, T_{melt} values of the population of lipids in the log stage might be expected to cluster together, creating one homogeneous phase (Fig. 3.10). In contrast, micron-scale phase separation occurs in membranes containing lipids with high T_{melt} values, lipids with low T_{melt} values, and a sterol (5–7). Therefore, one signature of phase separation could be a spreading of the T_{melt} values into a broader population (Fig. 3.10A). Or even a bifurcation of the T_{melt} values into two populations (Fig. 3.10B). One population

representative of the L_o phase, composed of low-T_{melt} lipids and one representative of the L_d phase, composed of high-T_{melt} lipids. For cumulative PC and PE data, our results were the opposite from this prediction. We found that in the log stage, there are lipids at high and low melting temperatures (Fig. 3.8). In the stationary stage, lipids in the population are more similar (one population) and at intermediate T_{melt} values.

Alternatively, if our sample is predominantly composed of the L_d phase, then we would expect to capture a shift in the lipid distribution to higher T_{melt} values (Fig. 3.10B). This lipidomic signature could also fit the scenario where phase separation is induced by the nucleation of the liquid ordered domain. We find a significant increase in the T_{melt} values for PC-lipids (Fig. 3.6). However, the combined PC and PE data paint a less clear picture. A challenge in the current study is that, at best, T_{melt} values have been measured or can be estimated for only ~50% of lipids. In addition, not all vacuoles have domains in the stationary stage, and it is likely that ~10-30% do not (16, 19, 29, 83). That means some fraction of our stationary sample may not have a composition representative of phase separation, potentially convoluting the lipidomic signature of phase separation.

Despite these challenges, we used known trends to inform how all the glycerolipids might affect the phase behavior of the membrane. We find that the most abundant lipids are increasing in T_{melt} (PC and PE) or likely have minimal effects (PI) (Fig. 3.9). Glycerolipids contributing to a decrease in T_{melt} are much less abundant (PS, PG, DAG). From the log to the stationary stage, the percent of glycerolipids with two saturated acyl decreases by 5%, and one unsaturated acyl chain increases by ~7% likely increasing T_{melt} of the membrane (Fig. 3.S9). This result is consistent with our prediction fromlipidomic signatures of phase separated membranes presented in Figure 3.10B, if we consider that our sample may be representative of the L_d phase or that phase separation is induced by an increase in lipids that partition to the L_d phase.

MATERIALS AND METHODS

Yeast cell culture

Saccharomyces cerevisiae BY4741 (78) harboring a Mam3-GFP translational fusion was used for the microscopy experiments. For the lipidomics experiments, *S. cerevisiae* BY4741 with a Mam3-myc-3c-3xFLAG was used. Cells were grown from a single colony on a plate, inoculated into 3 mL synthetic complete media for 20 hours. This starter culture was then diluted

to OD = 0.1 and grown at 30°C, shaken at 220 RPM. For yeast in the log stage, cells were grown for ~8 hours until the optical density (OD) = 1. For yeast in the stationary stage, cells were grown for 48 hours.

Microsomal preparation

To yield sufficient isolated vacuole membranes, 4,000 OD units were required. To reach this yield for the logarithmic growth, four one-liter cultures were inoculated. Cells were centrifuged at 3000 x g for 5 min at room temperature. The pellet was resuspended in 25 ml of pre-cooled PBS and placed on ice. Cells were then transferred to Falcon tubes, spun at 3000 x g for 5 min at 4°C. The supernatant was discarded. The pellet was snap frozen in liquid nitrogen and stored at -80°C.

Pellets were thawed from -80°C slowly on ice. The pellets were resuspended in 10 mL lysis buffer plus (25 mM HEPES pH 7.0, 1 mM EDTA, 0.6 M mannitol, added freshly: protease inhibitor cocktail and 1:40.000 benzonase). Cells are then transferred to pre-chilled Zirconia glass beads 0.5 mm diameter in a ratio of 1 OD units to 15 grams beads, and then the 15 mL falcon tube was overfilled to the top with lysis buffer plus to exclude air bubbles. Using a Fastprep shaker machine stored at 4°C, cells were shaken for 15 seconds at 5 m/s followed by 45 seconds of rest on ice to remove heat produced by shaking, repeated 10 times. The resulting lysate (supernatant w/o the beads) was transferred to fresh 15 mL tubes. A single wash of the beads with 6 mL lysis buffer plus is added to the saved supernatant.

Cell lysates were then spun at @ 3,234 x g for 5 minutes at 4°C. The supernatant was then transferred to a fresh 15 mL tube and re-centrifuge @ 3,234 g for 5 minutes at 4°C. The resulting supernatant is then transferred into ultracentrifuge tubes (polycarbonate bottles 26.3 ml, Beckman Coulter #355618), balanced using lysis buffer plus, and centrifuged (Ultracentrifuge Rotor Type 70 TI) at 11,973 x g at 4°C for 20 minutes. The resulting supernatant is transferred to a fresh ultracentrifuge tube, balanced with lysis buffer plus, and centrifuged 99,926 x g at 4°C for 60 minutes. To avoid lipid droplet contamination, a vacuum was used to suck off the supernatant in the ultracentrifuge tube, top down and a single wash with 15 mL of lysis buffer was performed. After discarding the supernatant, the pellet was resuspended in 1mL lysis buffer plus. The final product is then snap frozen in liquid nitrogen and stored at -80°C.

Pre-Immunoisolation preparation

Beads were prepared using a magnetic eppendorf tube holder. Dynabead Protein G for Immunoprecipitation (Thermo Fisher Scientific #10009D) was added to the number of Eppendorf tubes required for the preparation (1600 µL slurry / per 1000 OD culture). The supernatant was removed and the beads were washed by adding 1600 µL PBS-T (PBS, pH 7.4, 0.02 % (w/v) Tween-20) and resuspended by pipetting slowly. Beads were placed back in the magnetic holder and the supernatant was removed. Beads were finally resuspended in 1600 µL PBS-T and 10 µL of the anti-FLAG (M2, monoclonal mouse IgG1, affinity isolated antibody, F1804, 1 mg/ml) and left to rotate at 20 rpm overhead at 4°C overnight or in the morning for 1 hour at room temperature.

Immunoisolation preparation

Pellets from the microsomal preparation were thawed from -80°C slowly on ice. The preparation was then sonicated to break contact sites between organelles and to break vesicles into smaller, more homogenous sizes, a tip sonicator was used for 10 s, duty cycle 0.7 at 50% amplitude, on ice. The solution went from cloudy in appearance to clear. The sample was then centrifuged at 3,000 g at 4°C for 3 min. The supernatant is saved, while things that did not vesiculate are pelleted and removed.

Next we combined the antibody dyna beads with the vesicle preparation. The supernatant of the dyna magnetic beads was discarded and replaced with 800 µL of IP buffer (25 mM HEPES pH 7.0, 1 mM EDTA, 150 mM NaCl) and 800 µL of the sonicated supernatant to the beads for a total volume of 1600 µL. The sample was allowed to bind to the beads by rotating overhead at 2 rpm for 2 hours at 4°C.

To collect the beads with bound vacuole membrane vesicles, a series of washes were performed. First, the supernatant was removed utilizing the magnetic eppendorf tube rack. The bound beads were then washed two times with 1400 µL of wash buffer (25 mM HEPES pH 7.0, 1 mM EDTA, 75 mM NaCl, 0.6 M urea). Followed by two additional washes using 1400 µL IP buffer. The bound beads were finally resuspended in 500 µL of IP buffer and transferred to a new eppendorf tube.

To free the vesicles from the beads, the supernatant was removed and replaced with 500 µL of the elution buffer (PBS pH 7.4, 0.5 mM EDTA, 1 mM DTT, 0.04 mg/ml GST-3C protease, prepared freshly). The sample was mixed by rotating overhead at 2 rpm for 2 hours at 4°C. The samples were then placed in the magnet and the eluates (supernatant) were transferred to a new tube. Beads were kept to check the efficiency of the elution (Fig. 3.4).

Exchange the buffer for PBS (pH 7.4, filtered 0.22 µm) to remove protease and DTT for lipidomics. Mini ultracentrifuge tubes were rinsed with 1 mL PBS by vortex careful to avoid dust contamination. Eluates were transferred and combined in the UC-tubes. PBS buffer was used to fill and balance. The sample was centrifuged at 264,360 g for 2 hours at 4°C. Pour the supernatant out. In the case of a visible pellet, the residual liquid was vacuumed out and resuspended in 300 µL of the PBS buffer. In the case that the pellet is not visible, “resuspend” in the liquid left in the tube (~150 µL). The resuspended pellets were then transferred to eppendorf tubes, snap frozen in liquid nitrogen, and stored at -80°C. At each step in the procedure samples of the supernatant, pellet, etc. were saved for western blot analysis (see supplemental methods for more detail).

SUPPLEMENTAL FIGURES

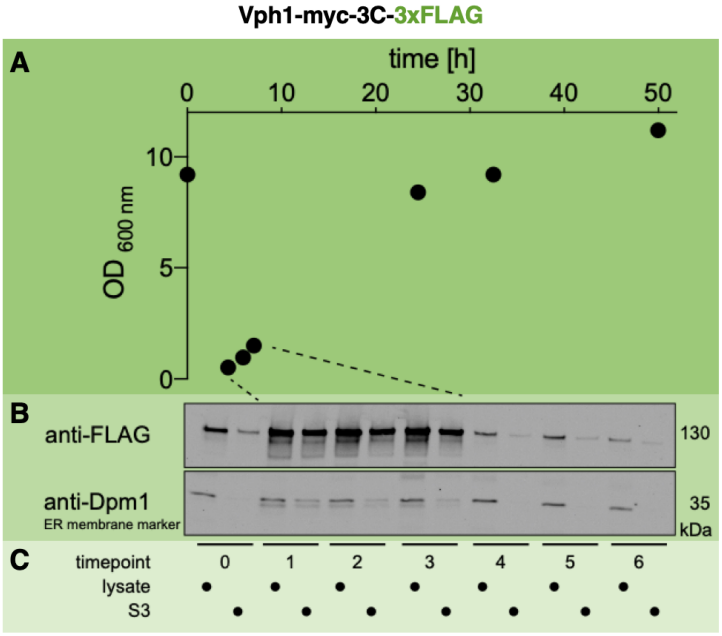

Figure 3.S1: (A) We tested 7 timepoints through the yeast growth cycle: The preculture at 19 hours of growth (0), the preculture was then diluted back to OD=0.1 and allowed to grow into the log (1-3), and stationary stage (4-6). **(C)** At each timepoint, we analyzed the cell lysate (first column in the gel for each timepoint, designated with a dot in row C), and the supernatant fraction after the first step in the microsome preparation, a 3,000 x g centrifugation (S3; second column in the gel for each timepoint, designated by a dot in row C). **(B)** The presence of Vph1 was visualized by staining for the FLAG tag attached to it. We find that in the log stage there is an abundance of Vph1 (timepoints 1-3) in the cell lysate and S3 samples. This result is consistent with the reported value of > 50,000 copies/cell which likely only applies to the log stage of growth (up to ~10 h of growth) (86, 102). In the stationary stage (timpoints 4-6), there is a significant reduction in Vph1 abundance in the cell lysate and a significant loss after the first centrifugation step (S3). Dpm1, an endoplasmic reticulum marker, is used as a control. Dpm1 is reported to have < 2,000 copies/cell and maintains the same abundance throughout the growth cycle (102).

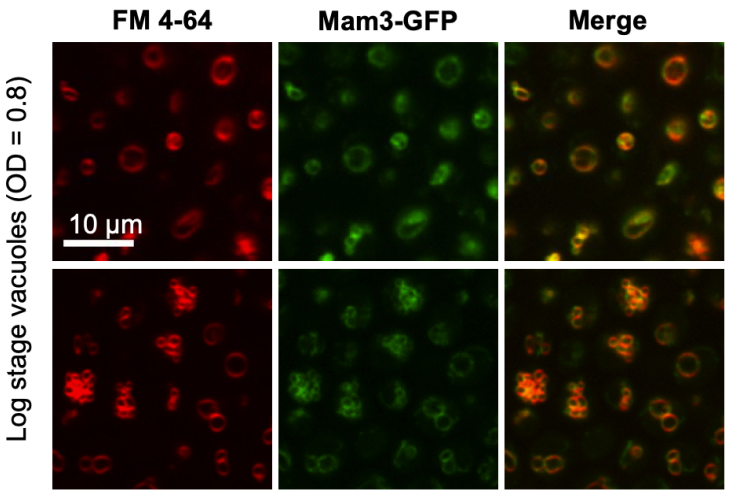

Figure 3.S2: The protein Mam3-GFP (middle column) colocalizes with FM 4-64 (left column), which is known to label vacuole membranes. All yeast in the field of view are living and are in the logarithmic stage; no micron-scale domains appear in their membranes. Images were taken at room temperature.

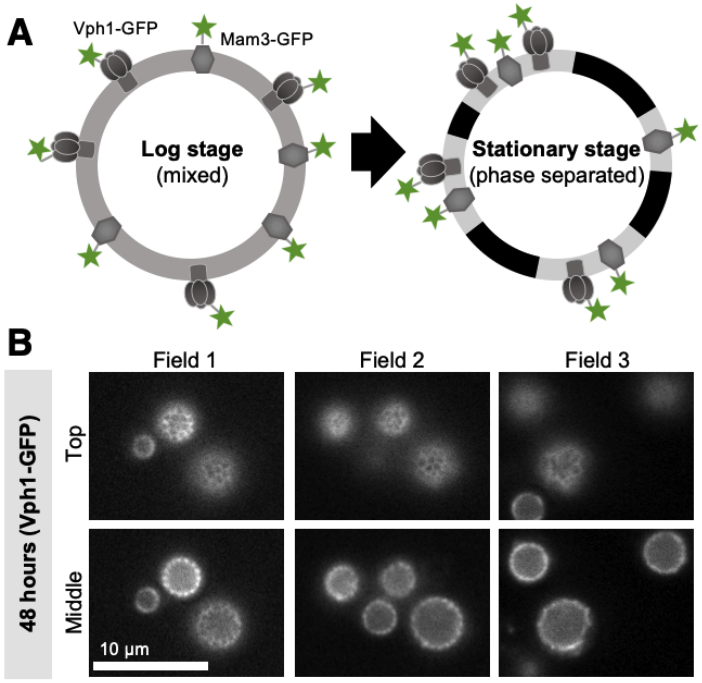

Figure 3.S3: (A) Left: For yeast in the logarithmic stage of growth, lipids and proteins appear uniformly distributed across the surface of vacuole membranes. Two of the proteins, Vph1 and Mam3, can be endogenously labeled with GFP (as shown here) or a bait tag for immunoisolation. **Right:** In the stationary stage, the membrane separates into two liquid phases. Vph1-GFP and Mam3-GFP preferentially partition to the same phase. **(B)** After 48 hours of growth, yeast are in the stationary stage of growth and most vacuole membranes have phase separated. The proteins Mam3 (Fig. 3.2) and Vph1 partition into only one of the phases, shown at both the top and the midplane of the vacuoles in each field of view. Images are of living cells and were taken at room temperature.

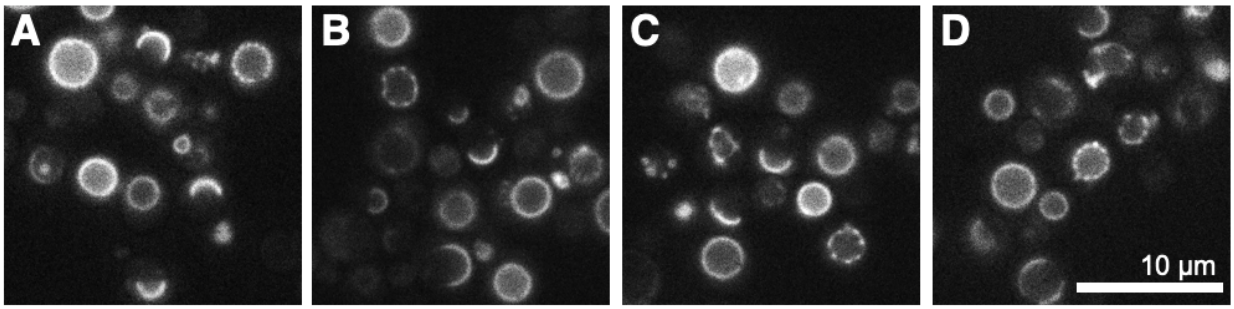

Figure 3.S4: Four fields of view of vacuole membranes in living yeast cells in the stationary stage after 48 hours of growth, under equivalent conditions. Bright areas of the membranes contain the fluorescent protein Mam3-GFP, which was endogenously labeled. Most membranes in the fields of view have phase-separated into micron-scale domains. Images were taken at room temperature.

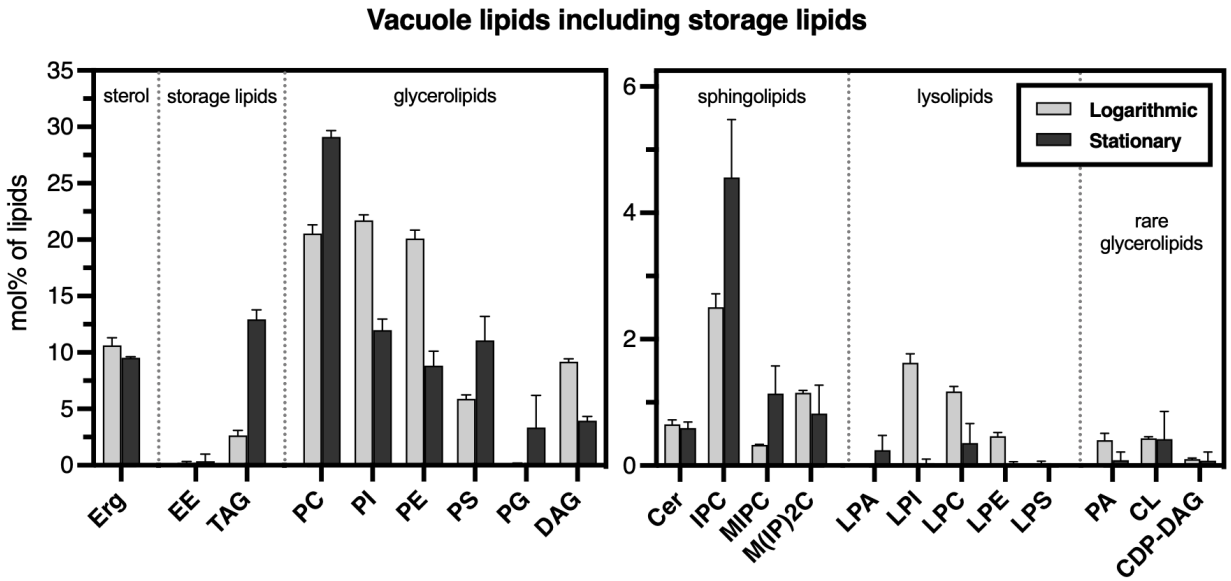

Figure 3.S5: All lipids in vacuole membranes isolated with a Mam3 bait tag as in Fig. S5. These data include the storage lipids of ergosterol esters (EE) and triacylglycerols (TAG). Acronyms of all other lipids are listed in Table 3.S1, below. LEFT: Most abundant lipid types. RIGHT: Less abundant lipid types. Note that the y-axis range is smaller in the graph at the right.

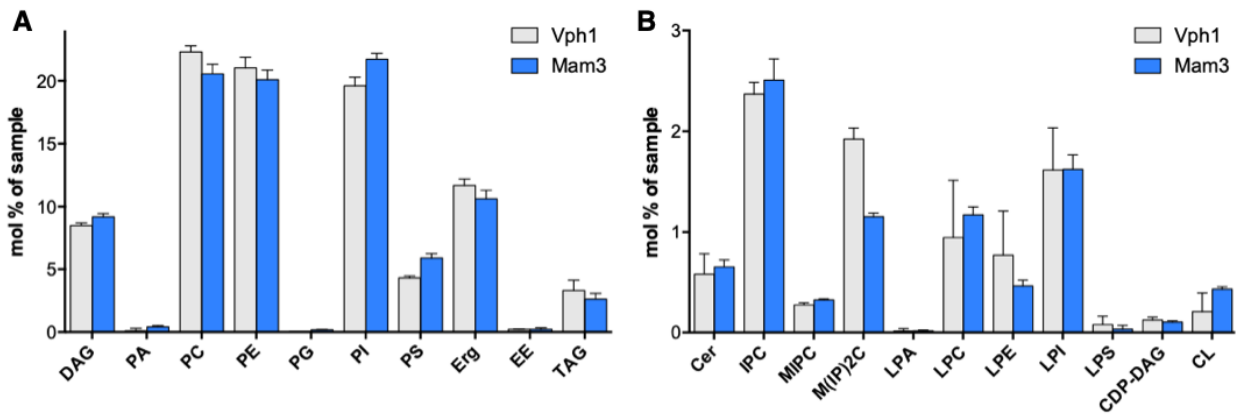

Figure 3.S6: Vacuole lipidome in the logarithmic stage using two different bait tags: Mam3 and Vph1. **(A)** Glycerolipids, sterol and storage lipids represent a majority of the lipidome. **(B)** Sphingolipids and ceramides are much less abundant (< 3 mol% of the lipidome). Overall, Mam3 derived immunoisolates from logarithmic cells are in good accordance with previous data collected using Vph1. However, there are differences in M(IP)2C and arguably also in PS levels. These might reflect real differences due to the different baits or experimental variation. The Vph1 data will be published in an accompanying manuscript (Reinhard et al. 2022).

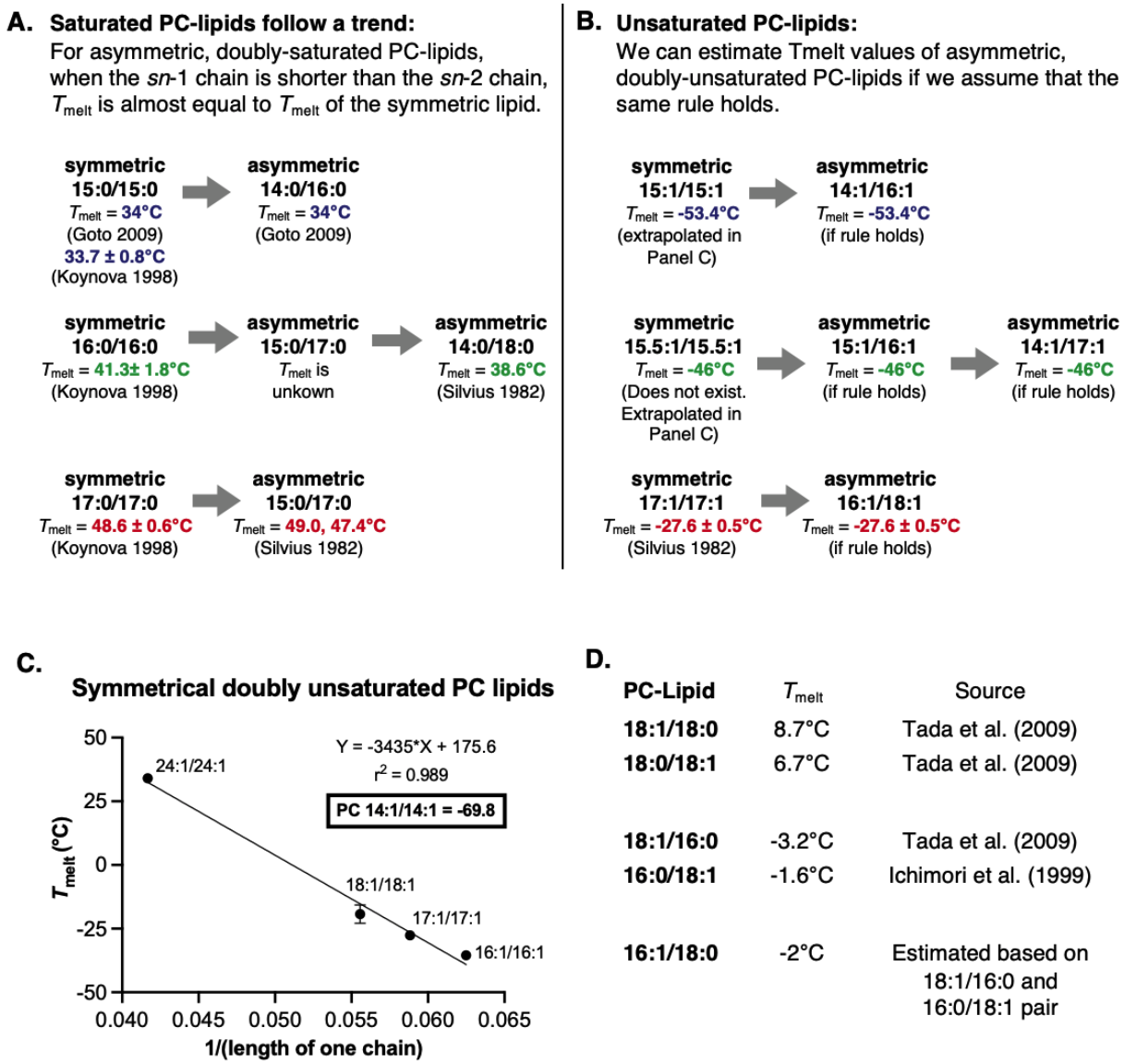

Figure 3.S7: Trends used to estimate melting temperatures for PC-lipids.

A. **Asymmetric lipids (n:0/18:1)**

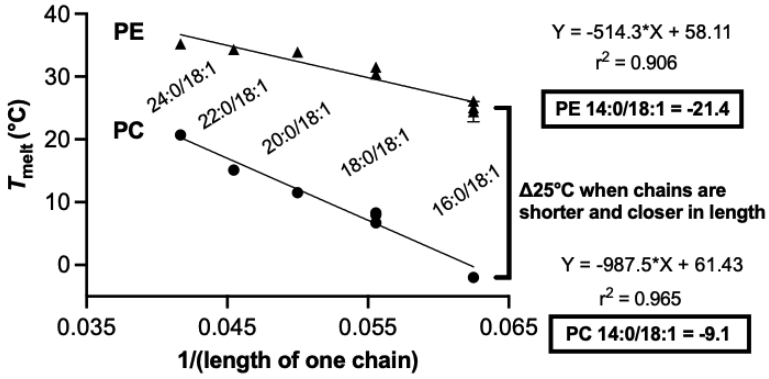

B. **PC lipids (n:0/n:1) symmetric or close in length**

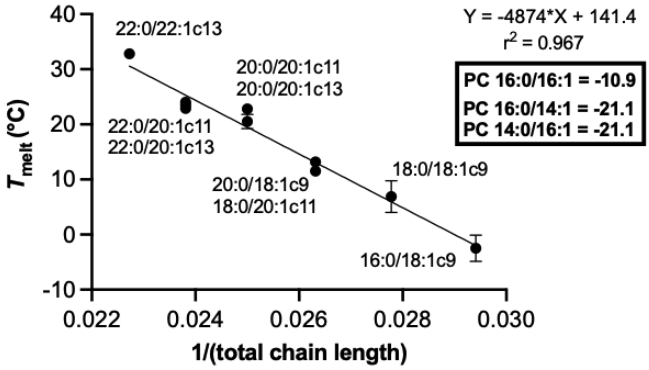

C.

Lipid	T_{melt}	Source
PE 16:1/16:1	-33.5°C	Koynova and Caffrey (1994)
PE 18:1/18:1	-16°C	Silvius (1982)
PE 16:1/18:1	-24.75°C	Estimated halfway in between 16:1/16:1 and 18:1/18:1
PC 16:0/16:1	-10.9°C	Extrapolated from F
PE 16:0/16:1	14.1°C	Estimated to be ~25°C higher than PC 16:0/16:1 based on difference in E where chains shorter and are closer in length
PE 16:0/18:1	25°C	Koynova and Caffrey (1994)
PE 14:0/18:1	21.4°C	Extrapolated from E
		(The difference between these is 3.6°C)
PE 16:0/16:1	14.1°C	Estimated above
PE 14:0/16:1	10.5°C	Estimated to be 3.6°C less

Figure 3.S8: Trends used to estimate melting temperatures for PE-lipids.

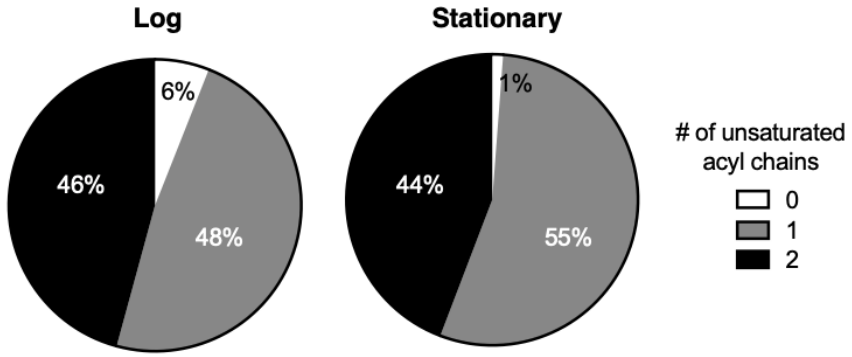

Figure 3.S9: Mol% of glycerolipids with 0, 1 or 2 unsaturated acyl chains. In the log stage there are more lipids with 1 unsaturated acyl chain and less lipids with doubly saturated acyl chains. However, these changes overall are quite small (~5-7%).

SUPPLEMENTARY TABLES

Acronym	Lipid Name
CDP-DAG	Cytidine diphosphate-diacylglycerol
Cer	Ceramide
CL	Cardiolipin
DAG	Diacylglycerol
EE	Ergosterol ester
Erg	Ergosterol
IPC	Inositol-phosphoryl-ceramide
LPA	Lysophosphatidic acid
LPC	Lysophosphatidylcholine
LPE	Lysophosphatidylethanolamine
LPI	Lysophosphatidylinositol
LPS	Lysophosphatidylserine
M(IP)2C	Mannosyl-diinositol-phosphoryl-ceramide
MIPC	Mannosyl-inositol-phosphoryl-ceramide
PA	Phosphatidic acid
PC	Phosphatidylcholine
PE	Phosphatidylethanolamine
PG	Phosphatidylglycerol
PI	Phosphatidylinositol
PS	Phosphatidylserine
TAG	Triacylglycerol

Table 3.S1: Acronyms for all lipids present in the yeast lipidome.

T_{melt} values for lipids in the vacuole membrane

PC Lipid:	T_{melt} (°C)	Source of T_{melt} value
14:1/14:1	-69.8	Extrapolated from graph (C)
14:1/16:1	-53.4	Estimated (B)
14:1/17:1	-53.4	Estimated (B)
15:1/16:1	-46.0	Estimated (B)
16:0/16:1	-10.9	Extrapolated (B)
16:0/18:1	-2.5 ± 2.4	Koynova & Caffrey (1998)
16:1/16:1	-35.5	Silvius (1982)
16:1/17:1	-32.6	Estimated (B)
16:1/18:0	-2	Estimated (D)
16:1/18:1	-27.5 ± 0.6	Silvius (1982)
18:0/18:1	6.7	Tada (2009)
18:1/18:1	-19.3 ± 3.6	Silvius (1982)

PE Lipid:	T_{melt} (°C)	Source of T_{melt} value
14:0/16:1	10.5	Estimated (F)
14:0/18:1	21.4	Extrapolated from graph (D)
16:0/16:1	14.1	Estimated (F)
16:0/18:1	25	Wang (1994)
16:1/16:1	-33.5	Koynova & Caffrey (1994)
16:1/18:1	19.5	Estimated (F)
18:0/18:1	30.4	Silvius (1982)
18:1/18:1	-5.5 ± 0.5	Matsuki et al. (2017)

Table 3.S2: Melting temperatures used to analyze the lipids present in the vacuole membrane. Many values were available in the literature. Those that were not, were estimated using known literature values and their trends (Table 3.S9)

Known T_{melt} values used to estimate vacuole lipids

Known PC-Lipids:	T_{melt} (°C)	Source of T_{melt} value
13:0/13:0	13.5	Silvius (1982)
14:0/14:0	24	Goto et al. (2009)
15:0/15:0	34 33.7 ± 0.8	Goto et al. (2009) Koynova & Caffrey (1998)
16:0/16:0	41.3± 1.8	Koynova & Caffrey (1998)
17:0/17:0	48.6 ± 0.6	Koynova & Caffrey (1998)
14:0/16:0	34	Goto et al. (2009)
14:0/18:0	38.6	Silvius (1982)
15:0/17:0	49.0, 47.4	Silvius (1982)
16:1/16:1	-35.5, -36°C	Silvius (1982)
17:1/17:1	-27.6 ± 0.5	(Silvius 1982)
18:1/18:1	-19.3 ± 3.6	(Silvius 1982)
24:1c9/24:1c9	34	Koynova & Caffrey (1998)
16:0/18:1	-1.6	Ichimori et al. (1999)
18:1/16:0	-3.2°C	Tada et al. (2009)
18:0/18:1	6.7	Tada et al. (2009)
18:1/18:0	8.7°C	Tada et al. (2009)
20:0/18:1	11.5 ± 0.5	Koynova & Caffrey (1998)
22:0/18:1	15.1	Koynova & Caffrey (1998)
24:0/18:1	20.7	Koynova & Caffrey (1998)
18:0/20:1c11	13.2	Koynova & Caffrey (1998)
20:00/20:1c11	20.5 ± 1.3	Koynova & Caffrey (1998)
20:00/20:1c13	22.8	Koynova & Caffrey (1998)
22:0/20:1c11	22.9	Koynova & Caffrey (1998)
22:0/20:1c13	23.5, 24	Koynova & Caffrey (1998)
22:0/22:1c13	32.8	Koynova & Caffrey (1998)

Known PE-Lipids:	T_{melt} (°C)	Source of T_{melt} value
16:0/18:1	24.41 ± 1.63, 26.1	Koynova & Caffrey (1994) Wang et al. (1994)
18:0/18:1	31.5 30.4	Wang et al. (1994) (Silvius, 1982)
20:0/18:1	33.9	Wang et al. (1994)
22:0/18:1	34.3	Wang et al. (1994)
24:0/18:1	35.2	Wang et al. (1994)
16:1/16:1	-33.5	Koynova & Caffrey (1994) Silvius (1982)
18:1/18:1	-5.5 ± 0.5	Matsuki et al. (2017)

Table 3.S3: Known literature values used to estimate unknown PC and PE melting temperatures.

Mol% of phospholipids in log stage (Total phospholipids = 100%)

Source	PC	PE	PI	PS	PA	Lyso	CL	Other	Method
Zinser 1991	*46.5*	*19.4*	*18.3*	*4.4*	*2.1*		*1.6*	*7.7*	*density gradient*
Tuller 1999	*39.2*	*26.6*	*24.4*	*3.9*	*2.5*	*1.6*	*0.4*	*1.4*	*density gradient*
Reinhard 2022	*31.4*	*29.6*	*27.6*	*6.1*	*0.2*	*4.8*	*0.3*		*immunoisolation*
This work	*28.3*	*27.7*	*29.9*	*8.1*	*0.6*	*4.6*	*0.6*	*.2 (PG)*	*immunoisolation*

Table 3.S4: Mol% of glycerolipids with 0, 1 or 2 unsaturated acyl chains. In the log stage there are more lipids with 1 unsaturated acyl chain and less lipids with doubly saturated acyl chains. However, these changes overall are quite small (~5-7%).

REFERENCES

1. O. G. Mouritsen, *Life - As a Matter of Fat: The Emerging Science of Lipidomics* (Springer Science & Business Media, 2006).

2. D. Marsh, Cholesterol-induced fluid membrane domains: a compendium of lipid-raft ternary phase diagrams. *Biochim. Biophys. Acta* **1788**, 2114–2123 (2009).

3. J. Hjort Ipsen, G. Karlström, O. G. Mourtisen, H. Wennerström, M. J. Zuckermann, Phase equilibria in the phosphatidylcholine-cholesterol system. *Biochimica et Biophysica Acta (BBA) - Biomembranes* **905**, 162–172 (1987).

4. S. L. Veatch, S. L. Keller, Seeing spots: complex phase behavior in simple membranes. *Biochim. Biophys. Acta* **1746**, 172–185 (2005).

5. S. L. Veatch, S. L. Keller, Miscibility phase diagrams of giant vesicles containing sphingomyelin. *Phys. Rev. Lett.* **94**, 148101 (2005).

6. S. L. Veatch, S. L. Keller, Organization in lipid membranes containing cholesterol. *Phys. Rev. Lett.* **89**, 268101 (2002).

7. G. W. Feigenson, J. T. Buboltz, Ternary phase diagram of dipalmitoyl-PC/dilauroyl-PC/cholesterol: nanoscopic domain formation driven by cholesterol. *Biophys. J.* **80**, 2775–2788 (2001).

8. L. A. Bagatolli, To see or not to see: lateral organization of biological membranes and fluorescence microscopy. *Biochim. Biophys. Acta* **1758**, 1541–1556 (2006).

9. S. L. Veatch, S. L. Keller, Separation of liquid phases in giant vesicles of ternary mixtures of phospholipids and cholesterol. *Biophys. J.* **85**, 3074–3083 (2003).

10. T. Baumgart, *et al.*, Large-scale fluid/fluid phase separation of proteins and lipids in giant plasma membrane vesicles. *Proc. Natl. Acad. Sci. U. S. A.* **104**, 3165–3170 (2007).

11. K. Simons, D. Toomre, Lipid rafts and signal transduction. *Nat. Rev. Mol. Cell Biol.* **1**, 31–39 (2000).

12. S. Munro, Lipid rafts: elusive or illusive? *Cell* **115**, 377–388 (2003).

13. K. Simons, M. J. Gerl, Revitalizing membrane rafts: new tools and insights. *Nat. Rev. Mol. Cell Biol.* **11**, 688–699 (2010).

14. D. Lingwood, K. Simons, Lipid rafts as a membrane-organizing principle. *Science* **327**, 46–50 (2010).

15. H. Moor, K. Muhlethaler, Fine structure in frozen-etched yeast cells. *J. Cell Biol.* **17**, 609–628 (1963).

16. A. Toulmay, W. A. Prinz, Direct imaging reveals stable, micrometer-scale lipid domains that segregate proteins in live cells. *J. Cell Biol.* **202**, 35–44 (2013).

17. A. Murley, *et al.*, Ltc1 is an ER-localized sterol transporter and a component of

ER–mitochondria and ER–vacuole contacts. *J. Cell Biol.* **209**, 539–548 (2015).

18. A. Murley, *et al.*, Sterol transporters at membrane contact sites regulate TORC1 and TORC2 signaling. *J. Cell Biol.* **216**, 2679–2689 (2017).

19. C.-W. Wang, Y.-H. Miao, Y.-S. Chang, A sterol-enriched vacuolar microdomain mediates stationary phase lipophagy in budding yeast. *J. Cell Biol.* **206**, 357–366 (2014).

20. A. Y. Seo, *et al.*, AMPK and vacuole-associated Atg14p orchestrate μ-lipophagy for energy production and long-term survival under glucose starvation. *Elife* **6**, e21690 (2017).

21. S. P. Rayermann, G. E. Rayermann, C. E. Cornell, A. J. Merz, S. L. Keller, Hallmarks of reversible separation of living, unperturbed cell membranes into two liquid phases. *Biophys. J.* **113**, 2425–2432 (2017).

22. C. P. Brangwynne, Phase transitions and size scaling of membrane-less organelles. *J. Cell Biol.* **203**, 875–881 (2013).

23. A. A. Hyman, C. A. Weber, F. Jülicher, Liquid-liquid phase separation in biology. *Annu. Rev. Cell Dev. Biol.* **30**, 39–58 (2014).

24. A. E. Posey, A. S. Holehouse, R. V. Pappu, Phase Separation of Intrinsically Disordered Proteins. *Methods Enzymol.* **611**, 1–30 (2018).

25. E. M. Langdon, A. S. Gladfelter, A New Lens for RNA Localization: Liquid-Liquid Phase Separation. *Annu. Rev. Microbiol.* **72**, 255–271 (2018).

26. S. F. Banani, H. O. Lee, A. A. Hyman, M. K. Rosen, Biomolecular condensates: organizers of cellular biochemistry. *Nat. Rev. Mol. Cell Biol.* **18**, 285–298 (2017).

27. C. H. Moeller, J. B. Mudd, W. W. Thomson, Lipid phase separations and intramembranous particle movements in the yeast tonoplast. *Biochimica et Biophysica Acta (BBA)-Biomembranes* **643**, 376–386 (1981).

28. C. H. Moeller, W. W. Thomson, An ultrastructural study of the yeast tonoplast during the shift from exponential to stationary phase. *J. Ultrastruct. Res.* **68**, 28–37 (1979).

29. T. Tsuji, *et al.*, Niemann-Pick type C proteins promote microautophagy by expanding raft-like membrane domains in the yeast vacuole. *Elife* **6**, e25960 (2017).

30. H. Alexandre, I. Rousseaux, C. Charpentier, Relationship between ethanol tolerance, lipid composition and plasma membrane fluidity in Saccharomyces cerevisiae and Kloeckera apiculata. *FEMS Microbiol. Lett.* **124**, 17–22 (1994).

31. K. M. You, C.-L. Rosenfield, D. C. Knipple, Ethanol Tolerance in the Yeast Saccharomyces cerevisiae Is Dependent on Cellular Oleic Acid Content. *Applied and Environmental Microbiology* **69**, 1499–1503 (2003).

32. S. Jackowski, Cell cycle regulation of membrane phospholipid metabolism. *J. Biol. Chem.* **271**, 20219–20222 (1996).

33. S. Spiegel, A. H. Merrill Jr, Sphingolipid metabolism and cell growth regulation. *FASEB J.* **10**, 1388–1397 (1996).

34. G. E. Atilla-Gokcumen, *et al.*, Dividing Cells Regulate Their Lipid Composition and Localization. *Cell* **156**, 428–439 (2014).

35. M. Ponec, A. Weerheim, J. Kempenaar, A. M. Mommaas, D. H. Nugteren, Lipid composition of cultured human keratinocytes in relation to their differentiation. *J. Lipid Res.* **29**, 949–961 (1988).

36. N. M. Gulaya, G. L. Volkov, V. M. Klimashevsky, N. N. Govseeva, A. A. Melnik, Changes in lipid composition of neuroblastoma C1300 N18 cell during differentiation. *Neuroscience* **30**, 153–164 (1989).

37. E. M. Gray, G. Díaz-Vázquez, S. L. Veatch, Growth Conditions and Cell Cycle Phase Modulate Phase Transition Temperatures in RBL-2H3 Derived Plasma Membrane Vesicles. *PLOS ONE* **10**, e0137741 (2015).

38. E. Cammarota, *et al.*, Criticality of plasma membrane lipids reflects activation state of macrophage cells. *J. R. Soc. Interface* **17**, 20190803 (2020).

39. M. J. Tisza, *et al.*, Motility and stem cell properties induced by the epithelial-mesenchymal transition require destabilization of lipid rafts. *Oncotarget* **7**, 51553–51568 (2016).

40. C. R. Santos, A. Schulze, Lipid metabolism in cancer. *FEBS J.* **279**, 2610–2623 (2012).

41. R. G. Cutler, *et al.*, Involvement of oxidative stress-induced abnormalities in ceramide and cholesterol metabolism in brain aging and Alzheimer's disease. *Proceedings of the National Academy of Sciences* **101**, 2070–2075 (2004).

42. M. Maes, *et al.*, Fatty acid composition in major depression: decreased ω3 fractions in cholesteryl esters and increased C20:4ω6C20:5ω3 ratio in cholesteryl esters and phospholipids. *Journal of Affective Disorders* **38**, 35–46 (1996).

43. R. Ernst, C. S. Ejsing, B. Antonny, Homeoviscous Adaptation and the Regulation of Membrane Lipids. *J. Mol. Biol.* **428**, 4776–4791 (2016).

44. K. Hunter, A. H. Rose, Influence of Growth Temperature on the Composition and Physiology of Micro-organisms. *Environmental Control of Cell Synthesis and Function*, 527–540 (1972).

45. M. Kates, R. M. Baxter, Lipid composition of mesophilic and psychrophilic yeasts (Candida species) as influenced by environmental temperature. *Can. J. Biochem. Physiol.* **40**, 1213–1227 (1962).

46. J. Farrell, A. Rose, Temperature Effects on Microorganisms. *Annual Review of Microbiology* **21**, 101–120 (1967).

47. M. Burns, K. Wisser, J. Wu, I. Levental, S. L. Veatch, Miscibility transition temperature scales with growth temperature in a zebrafish cell line. *Biophys. J.* **113**, 1212–1222 (2017).

48. B. B. Machta, *et al.*, Conditions that Stabilize Membrane Domains Also Antagonize n-Alcohol Anesthesia. *Biophysical Journal* **111**, 537–545 (2016).

49. B. B. Machta, S. Papanikolaou, J. P. Sethna, S. L. Veatch, Minimal model of plasma membrane heterogeneity requires coupling cortical actin to criticality. *Biophys. J.* **100**,

1668–1677 (2011).

50. J. Ehrig, E. P. Petrov, P. Schwille, Near-critical fluctuations and cytoskeleton-assisted phase separation lead to subdiffusion in cell membranes. *Biophys. J.* **100**, 80–89 (2011).

51. M. E. Beattie, S. L. Veatch, B. L. Stottrup, S. L. Keller, Sterol structure determines miscibility versus melting transitions in lipid vesicles. *Biophys. J.* **89**, 1760–1768 (2005).

52. A. V. Samsonov, I. Mihalyov, F. S. Cohen, Characterization of cholesterol-sphingomyelin domains and their dynamics in bilayer membranes. *Biophys. J.* **81**, 1486–1500 (2001).

53. T. M. Konyakhina, J. Wu, J. D. Mastroianni, F. A. Heberle, G. W. Feigenson, Phase diagram of a 4-component lipid mixture: DSPC/DOPC/POPC/chol. *Biochim. Biophys. Acta* **1828**, 2204–2214 (2013).

54. S. L. Veatch, K. Gawrisch, S. L. Keller, Closed-loop miscibility gap and quantitative tie-lines in ternary membranes containing diphytanoyl PC. *Biophys. J.* **90**, 4428–4436 (2006).

55. A. Y. Seo, *et al.*, Vacuole phase-partitioning boosts mitochondria activity and cell lifespan through an inter-organelle lipid pipeline. *bioRxiv*, 2021.04.11.439383 (2021).

56. F. Spira, *et al.*, Patchwork organization of the yeast plasma membrane into numerous coexisting domains. *Nat. Cell Biol.* **14**, 640–648 (2012).

57. L. Wang, E. S. Seeley, W. Wickner, A. J. Merz, Vacuole fusion at a ring of vertex docking sites leaves membrane fragments within the organelle. *Cell* **108**, 357–369 (2002).

58. C. E. Cornell, *et al.*, n-Alcohol Length Governs Shift in Lo-Ld Mixing Temperatures in Synthetic and Cell-Derived Membranes. *Biophys. J.* **113**, 1200–1211 (2017).

59. J. Zhao, J. Wu, S. L. Veatch, Adhesion Stabilizes Robust Lipid Heterogeneity in Supercritical Membranes at Physiological Temperature. *Biophysical Journal* **104**, 825–834 (2013).

60. V. D. Gordon, M. Deserno, C. M. J. Andrew, S. U. Egelhaaf, W. C. K. Poon, Adhesion promotes phase separation in mixed-lipid membranes. *EPL (Europhysics Letters)* **84**, 48003 (2008).

61. R. Lipowsky, T. Rouhiparkouhi, D. E. Discher, T. R. Weikl, Domain formation in cholesterol–phospholipid membranes exposed to adhesive surfaces or environments. *Soft Matter* **9**, 8438 (2013).

62. R. Schneiter, *et al.*, Electrospray ionization tandem mass spectrometry (ESI-MS/MS) analysis of the lipid molecular species composition of yeast subcellular membranes reveals acyl chain-based sorting/remodeling of distinct molecular species en route to the plasma membrane. *J. Cell Biol.* **146**, 741–754 (1999).

63. E. Zinser, F. Paltauf, G. Daum, Sterol composition of yeast organelle membranes and subcellular distribution of enzymes involved in sterol metabolism. *J. Bacteriol.* **175**, 2853–2858 (1993).

64. E. Sezgin, I. Levental, S. Mayor, C. Eggeling, The mystery of membrane organization: composition, regulation and roles of lipid rafts. *Nat. Rev. Mol. Cell Biol.* **18**, 361–374 (2017).

65. I. Levental, S. L. Veatch, The continuing mystery of lipid rafts. *J. Mol. Biol.* **428**, 4749–4764 (2016).

66. M. L. Kraft, Sphingolipid organization in the plasma membrane and the mechanisms that influence it. *Frontiers in cell and developmental biology* **4**, 154 (2017).

67. E. Klotzsch, G. J. Schütz, A critical survey of methods to detect plasma membrane rafts. *Philos. Trans. R. Soc. Lond. B Biol. Sci.* **368**, 20120033 (2013).

68. I. Levental, *et al.*, Cholesterol-dependent phase separation in cell-derived giant plasma-membrane vesicles. *Biochem. J* **424**, 163–167 (2009).

69. M. Hao, S. Mukherjee, F. R. Maxfield, Cholesterol depletion induces large scale domain segregation in living cell membranes. *Proc. Natl. Acad. Sci. U. S. A.* **98**, 13072–13077 (2001).

70. S. Mahammad, J. Dinic, J. Adler, I. Parmryd, Limited cholesterol depletion causes aggregation of plasma membrane lipid rafts inducing T cell activation. *Biochim. Biophys. Acta* **1801**, 625–634 (2010).

71. C. Klose, *et al.*, Flexibility of a Eukaryotic Lipidome – Insights from Yeast Lipidomics. *PLoS ONE* **7**, e35063 (2012).

72. T. Tsuji, T. Fujimoto, Lipids and lipid domains of the yeast vacuole. *Biochem. Soc. Trans.* **46**, 1047–1054 (2018).

73. C. H. Moeller, W. W. Thomson, Uptake of lipid bodies by the yeast vacuole involving areas of the tonoplast depleted of intramembranous particles. *Journal of Ultrastructure Research* **68**, 38–45 (1979).

74. A. Yamamoto, *et al.*, Novel PI(4)P 5-kinase homologue, Fab1p, essential for normal vacuole function and morphology in yeast. *Mol. Biol. Cell* **6**, 525–539 (1995).

75. Y. Kamada, U. S. Jung, J. Piotrowski, D. E. Levin, The protein kinase C-activated MAP kinase pathway of Saccharomyces cerevisiae mediates a novel aspect of the heat shock response. *Genes Dev.* **9**, 1559–1571 (1995).

76. C.-J. Huang, M.-Y. Lu, Y.-W. Chang, W.-H. Li, Experimental Evolution of Yeast for High-Temperature Tolerance. *Mol. Biol. Evol.* **35**, 1823–1839 (2018).

77. D. Lockshon, *et al.*, Rho signaling participates in membrane fluidity homeostasis. *PLoS One* **7**, e45049 (2012).

78. C. B. Brachmann, *et al.*, Designer deletion strains derived from Saccharomyces cerevisiae S288C: a useful set of strains and plasmids for PCR-mediated gene disruption and other applications. *Yeast* **14**, 115–132 (1998).

79. T. Boothe, *et al.*, A tunable refractive index matching medium for live imaging cells, tissues and model organisms. *Elife* **6** (2017).

80. C. E. Cornell, *et al.*, Tuning Length Scales of Small Domains in Cell-Derived Membranes and Synthetic Model Membranes. *Biophys. J.* **115**, 690–701 (2018).

81. M. I. Angelova, S. Soléau, P. Méléard, F. Faucon, P. Bothorel, Preparation of giant vesicles by external AC electric fields. Kinetics and applications in *Trends in Colloid and Interface Science VI*, (Steinkopff, 1992), pp. 127–131.

82. C. R. Burtner, C. J. Murakami, B. K. Kennedy, M. Kaeberlein, A molecular mechanism of chronological aging in yeast. *Cell Cycle* **8**, 1256–1270 (2009).

83. C. L. Leveille, C. E. Cornell, A. J. Merz, S. L. Keller, Yeast cells actively tune their membranes to phase separate at temperatures that scale with growth temperatures. *bioRxiv*, 2021.09.14.460156 (2021).

84. X. Pan, *et al.*, Nucleus–Vacuole Junctions in Saccharomyces cerevisiae Are Formed Through the Direct Interaction of Vac8p with Nvj1p. *MBoC* **11**, 2445–2457 (2000).

85. A. Franzusoff, E. Lauzé, K. E. Howell, Immuno-isolation of Sec7p-coated transport vesicles from the yeast secretory pathway. *Nature* **355**, 173–175 (1992).

86. B. Ho, A. Baryshnikova, G. W. Brown, Unification of Protein Abundance Datasets Yields a Quantitative Saccharomyces cerevisiae Proteome. *Cell Syst* **6**, 192–205.e3 (2018).

87. W.-K. Huh, *et al.*, Global analysis of protein localization in budding yeast. *Nature* **425**, 686–691 (2003).

88. T. van Zutphen, *et al.*, Lipid droplet autophagy in the yeast Saccharomyces cerevisiae. *Mol. Biol. Cell* **25**, 290–301 (2014).

89. J. A. Hamilton, D. M. Small, Solubilization and localization of triolein in phosphatidylcholine bilayers: a 13C NMR study. *Proc. Natl. Acad. Sci. U. S. A.* **78**, 6878–6882 (1981).

90. P. J. Spooner, D. M. Small, Effect of free cholesterol on incorporation of triolein in phospholipid bilayers. *Biochemistry* **26**, 5820–5825 (1987).

91. R. Koynova, M. Caffrey, Phases and phase transitions of the phosphatidylcholines. *Biochim. Biophys. Acta* **1376**, 91–145 (1998).

92. J. R. Silvius, Thermotropic phase transitions of pure lipids in model membranes and their modifications by membrane proteins. *Lipid-protein interactions* **2**, 239–281 (1982).

93. K. Tada, *et al.*, Barotropic and thermotropic bilayer phase behavior of positional isomers of unsaturated mixed-chain phosphatidylcholines. *Biochim. Biophys. Acta* **1788**, 1056–1063 (2009).

94. H. Ichimori, T. Hata, H. Matsuki, S. Kaneshina, Effect of unsaturated acyl chains on the thermotropic and barotropic phase transitions of phospholipid bilayer membranes. *Chem. Phys. Lipids* **100**, 151–164 (1999).

95. M. Goto, S. Ishida, N. Tamai, H. Matsuki, S. Kaneshina, Chain asymmetry alters thermotropic and barotropic properties of phospholipid bilayer membranes. *Chem. Phys. Lipids* **161**, 65–76 (2009).

96. Z. Q. Wang, H. N. Lin, S. Li, C. H. Huang, Calorimetric studies and molecular mechanics simulations of monounsaturated phosphatidylethanolamine bilayers. *J. Biol. Chem.* **269**, 23491–23499 (1994).

97. R. Koynova, M. Caffrey, Phases and phase transitions of the hydrated phosphatidylethanolamines. *Chem. Phys. Lipids* **69**, 1–34 (1994).

98. H. Matsuki, *et al.*, Thermotropic and barotropic phase transitions on diacylphosphatidylethanolamine bilayer membranes. *Biochim. Biophys. Acta Biomembr.* **1859**, 1222–1232 (2017).

99. G. Tuller, T. Nemec, C. Hrastnik, G. Daum, Lipid composition of subcellular membranes of an FY1679-derived haploid yeast wild-type strain grown on different carbon sources. *Yeast* **15**, 1555–1564 (1999).

100. E. Uchida, Y. Ohsumi, Y. Anraku, [41] Purification of yeast vacuolar membrane H -ATPase and enzymological discrimination of three ATP-driven proton pumps in Saccharomyces cerevisiae. *Methods in Enzymology*, 544–562 (1988).

101. S. L. Veatch, I. V. Polozov, K. Gawrisch, S. L. Keller, Liquid domains in vesicles investigated by NMR and fluorescence microscopy. *Biophys. J.* **86**, 2910–2922 (2004).

102. S. Ghaemmaghami, *et al.*, Global analysis of protein expression in yeast. *Nature* **425**, 737–741 (2003).